Materials Horizons

Accepted Manuscript

This article can be cited before page numbers have been issued, to do this please use: S. Li, Z. Zhu, Y. Zhang, Y. Liu, X. Zhang and K. N. Hui, *Mater. Horiz.*, 2025, DOI: 10.1039/D5MH00221D.




ROYAL SOCIETY OF CHEMISTRY

rsc.li/materials-horizons

View Article Online
DOI: 10.1039/D5MH00221D

## Wider Impact Statement

The sustainable production of hydrogen peroxide ($H_2O_2$) is pivotal for a broad range of industrial and environmental applications, yet its current large-scale synthesis via the anthraquinone process remains energy-intensive and environmentally taxing. This review highlights recent advances in carbon-based electrocatalysts for decentralized, electrochemical $H_2O_2$ generation—a promising alternative that operates under mild conditions with minimal environmental footprint. The development of efficient, stable, and cost-effective carbon-based materials for electrochemical $H_2O_2$ production has profound implications for sustainable chemical manufacturing, decentralized wastewater treatment, and green energy applications. By providing a comprehensive analysis of cutting-edge catalyst engineering strategies, mechanistic insights, and structure-performance relationships, this work lays the foundation for the rational design of next-generation carbon-based electrocatalysts. Additionally, this review underscores critical challenges and future research directions, serving as a valuable roadmap for the transition toward scalable, eco-friendly $H_2O_2$ synthesis. The insights presented herein will not only advance fundamental scientific understanding but also accelerate practical implementation in industrial and environmental sectors.



View Article Online
DOI: 10.1039/D5MH00221D

## Data Availability Statement

No new experimental data were generated in this study. All data supporting the findings of this review are available in the cited literature and references within the manuscript.



# Innovative Engineering Strategies and Mechanistic Insights for Enhanced Carbon-Based Electrocatalysts in Sustainable $H_2O_2$ Production

Shun Li,[*a] Zhanpeng Zhu, [a] Yuqiao Zhang,[a] Yong Liu[b], Xinyue Zhang[*ab] and Kwun Nam Hui[*c]

[a] Institute of Quantum and Sustainable Technology (IQST), School of Chemistry and Chemical Engineering, Jiangsu University, Zhenjiang, 212013, China.
E-mail: shun@ujs.edu.cn

[b] Foshan (Southern China) Institute for New Materials, Foshan, 528200, China.
E-mail: zhangxinyue@fscinm.com

[c] Joint Key Laboratory of the Ministry of Education, Institute of Applied Physics and Materials Engineering, University of Macau, Avenida da Universidade, Taipa, Macau SAR, China
E-mail: bizhui@um.edu.mo



View Article Online
DOI: 10.1039/D5MH00221D

**Abstract:** Hydrogen peroxide ($H_2O_2$) plays a crucial role in various industrial sectors and everyday applications. Given the energy-intensive nature of the current anthraquinone process for its production, the quest for cost-effective, efficient, and stable catalysts for $H_2O_2$ synthesis is paramount. A promising sustainable approach lies in small-scale, decentralized electrochemical methods. Carbon nanomaterials have emerged as standout candidates, offering low costs, high surface areas, excellent conductivity, and adjustable electronic properties. This review presents a thorough examination of recent strides in engineering strategies of carbon-based nanomaterials for enhanced electrochemical $H_2O_2$ generation. It delves into tailored microstructures (e.g., 1D, 2D, porous architectures), defect/surface engineering (e.g., edge sites, heteroatom doping, surface modification), and heterostructure assembly (e.g., semiconductor-carbon composites, single-atom, dual-single-atom catalysts). Moreover, the review explores structure-performance interplays in these carbon electrocatalysts, drawing from advanced experimental analyses and theoretical models to unveil the mechanisms governing selective electrocatalytic $H_2O_2$ synthesis. Lastly, this review identifies challenges and charts future research avenues to propel carbon electrocatalysts towards greener and more effective $H_2O_2$ production methods.

**Keywords:** Hydrogen peroxide; electrocatalysts; carbon nanomaterials; materials engineering

View Article Online
DOI: 10.1039/D5MH00221D



## 1. Introduction

Hydrogen peroxide ($H_2O_2$) is an essential and environmentally friendly chemical with indispensable roles in various industrial applications, including electronics, chemical synthesis, medicine, wastewater treatment, bleaching processes, and environmental remediation.[1-4] Traditionally, industrial $H_2O_2$ production (~95%) is predominantly achieved through the energy-intensive anthraquinone process,[5, 6] which involves complex reaction steps, requires toxic solvents under harsh conditions, and generates substantial organic waste, posing significant environmental challenges. These drawbacks have stimulate considerable interest in developing on-site, environmentally benign, energy-efficient, and cost-effective methods for $H_2O_2$ production, including direct synthesis using $H_2$ and $O_2$,[7, 8] photocatalysis,[9-20] electrocatalysis,[21-28] mechanocatalysis,[29-32] and thermoelectrocatalysis.[33-35] Among these alternatives, electrochemical synthesis of $H_2O_2$ is particularly promising because it operates under mild conditions, requiring only electricity, air, and inexpensive electrolytes, while enabling high efficiency and decentralized production.[36, 37] However, achieving high selectivity for the $2e^-$ reduction pathway to produce $H_2O_2$, instead of the $4e^-$ pathway for producing water, is critical for this process.[38, 39] While noble-metal Pt- and Pd-based alloys have demonstrated excellent performance,[24, 40, 41] the scarcity and high cost severely limit their practical applications. Therefore, there is increasing interest in developing noble-metal-free electrocatalysts with high-efficiency and selectivity for $H_2O_2$ production.

Since the pioneering work on nitrogen-doped carbon nanotubes for efficient electrochemical oxygen reduction reaction (ORR) in 2009,[42] carbon-based metal-free electrocatalysts have garnered considerable research attention.[43, 44] Various carbon nanomaterials, such as graphene,[45] carbon nanotubes (CNTs),[46] carbon nanofibers/wires,[47] carbon dots,[48] fullerene,[49] and porous carbon,[50] have demonstrated great potential as catalysts for electrochemical production of $H_2O_2$ via $2e^-$ ORR pathway.[51] These materials offer great advantages like low cost, abundant availability, tunable nanostructure, excellent electrical conductivity, and

View Article Online
DOI: 10.1039/D5MH00221D

adjustable electronic properties.[52, 53] However, several challenges remain in optimizing these catalysts for $H_2O_2$ production, including 1) high overpotential, low catalytic activity and selectivity compared to precious metal catalysts; 2) unclear mechanisms involving active sites and reaction pathways; 3) poor stability and durability in acidic or alkaline environments; 4) integration with electrochemical systems for scalable production.

To overcome these inherent limitations, many strategies have been developed in the past few decades. Several important review papers have been published on carbon-based nanomaterials for $H_2O_2$ production.[53-57] As a rapidly growing field, recent studies have demonstrated notable advancements in the rational design and fabrication of carbon-based electrocatalysts. Moving beyond traditional catalyst optimization methods, innovative engineering strategies have been developed, such as precise modulation of microstructures (e.g., programed hierarchical structure), multi-component synergistic engineering (e.g., topological and doping effect), and the incorporation of atomically precise catalytic centers (e.g. dual-single-atom sites). These modification strategies have led to significantly enhanced $H_2O_2$ production activity, selectivity and stability, achieving performance levels that rival or even surpass those of the leading catalysts reported to date. Therefore, it is timely to provide a comprehensive overview of the latest breakthroughs in advanced engineering strategies of carbon-based nanomaterials in electrochemical $H_2O_2$ production (**Figure 1**). First, we describe the mechanisms of the $2e^-$ ORR and water oxidation reaction (WOR) pathways and elucidate the key factors influencing selectivity and activity. Next, we thoroughly summarize the recent progress in carbon-based electrocatalysts for $H_2O_2$ synthesis, emphasizing their underlying structure-performance relationships, particularly in the $2e^-$ ORR pathway. Finally, we highlight the current challenges and propose future directions for the rational design and large-scale utilization of advanced carbon-based electrocatalytic materials.

View Article Online
DOI: 10.1039/D5MH00221D



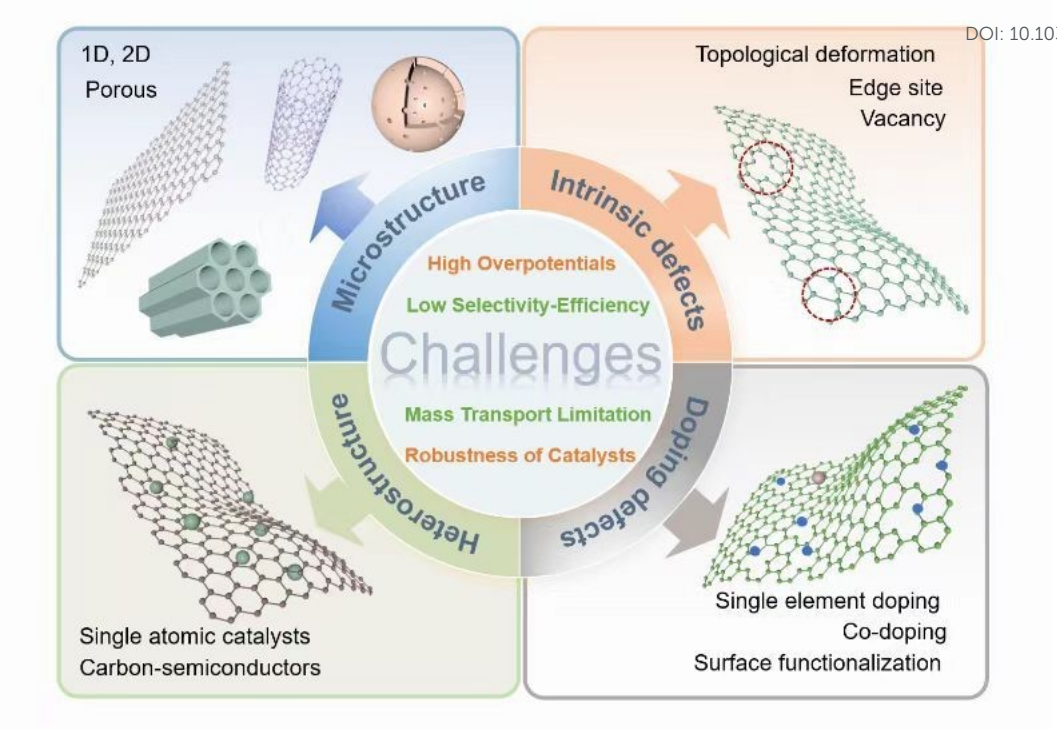


**Figure 1.** Schematics of key challenges and corresponding modification strategies of carbon-based electrocatalysts for $H_2O_2$ production.

## 2. Fundamentals of electrochemical $H_2O_2$ production

Electrocatalytic $H_2O_2$ production can be achieved through both ORR and WOR (**Figure 2**). These processes involve multi-electron reactions characterized by several elementary steps and potential intermediates (e.g., *OOH and *OH).[58, 59] The mechanisms of the ORR and WOR reactions are presented below in detail.

### 2.1. Two-electron pathway via Oxygen Reduction Reaction (ORR)

Generally, ORR involves a complex multi-electron transfer process, which can be categorized as dissociative and associative mechanisms. For the dissociative mechanism, the O−O bond in the adsorbed $O_2$ cleaves directly, resulting in the formation of $O_{ads}$ and $H_2O$ as the final product. In contrast, the associative mechanism involves the couple of adsorbed $O_2$ with an electron ($e^-$) and a proton ($H^+$) to form the *OOH intermediate,[60] which can further accept another $e^-$ and $H^+$ to produce $H_2O_2$. Additionally, the O−O bond in the *OOH intermediate may also dissociate, yielding $O_{ads}$ and $OH_{ads}$ and ultimately leading to the

View Article Online
DOI: 10.1039/D5MH00221D

formation of $H_2O$ (*OOH + $H^+$ + $e^-$ → *O + $H_2O$).[61] Thus, $H_2O_2$ is obtained as the main product by intervening in the dissociation of the peroxide species from the surface, as shown in Equations 1 and 2.[62, 63] Thus, the two competitive reactions involving the *OOH intermediate determine the selectivity for $H_2O_2$ generation.

$$O_2 + * + H^+ + e^- \rightarrow *OOH \quad (1)$$

$$*OOH + H^+ + e^- \rightarrow H_2O_2 + * \quad (2)$$

Consequently, ORR mechanisms can be divided into two pathways: the $2e^-$ or $4e^-$ pathway. The $4e^-$ pathway is preferred as the cathode reaction in fuel cells and metal-air batteries to obtain higher voltage and energy efficiency, while the electrochemical production of $H_2O_2$ relies on the $2e^-$ pathway (Equations 3 and 4).

In acidic medium:

$$O_2 + 2H^+ + 2e^- \rightarrow H_2O_2 \ (E^0 = 0.67\ V_{RHE}) \quad (3)$$

In alkaline medium (pH > 11.6):

$$O_2 + H_2O + 2e^- \rightarrow HO_2^- + OH^- \ (E^0 = 0.76\ V_{RHE}) \quad (4)$$

A critical aspect in determining the pathway of the ORR is the adsorption mode of $O_2$ molecules on the catalyst's surface. In paricular, when $O_2$ is adsorbed in the Pauling mode, the O−O bond is less likely to break, thus favoring $H_2O_2$ generation.[64]

### 2.2. Two-electron pathway via Water Oxidation Reaction (WOR)

The WOR process can occur through $1e^-$, $2e^-$, and $4e^-$ oxidative pathways and $H_2O_2$ can be generated via the $2e^-$ pathway, while the complete oxidation pathway to $O_2$ needs to be avoided ($2H_2O + 2H^+ + 2e^- \rightarrow O_2$).[65-67] The specific WOR steps by $2e^-$ pathway for $H_2O_2$ production are as follows:

$$2H_2O \rightarrow H_2O_2 + 2H^+ + 2e^- \ (E^0 = 1.76\ V_{RHE}) \quad (5)$$

View Article Online
DOI: 10.1039/D5MH00221D

$$* + H_2O \rightarrow *OH + H^+ + e^- \quad (6)$$

$$*OH + *OH \rightarrow H_2O_2 \quad (7)$$

The key issue for determining the pathway of the WOR is the recombination of *OH species on the catalyst's surface. Specifically, if *OH is not further oxidized to *O or •OH, $H_2O_2$ generation is favored.

### 2.3. Mechanistic insights into electrochemical $H_2O_2$ production

In the electrocatalytic production of $H_2O_2$ via the ORR and WOR mechanisms, the key factors determining efficiency and selectivity mainly include catalyst materials and elctrolyte properties. Catalysts with optimized surface electronic structures, such as those exhibiting moderate adsorption energies for oxygen intermediates (e.g., *OOH), favor the $2e^-$ pathway with low overpotential. Additionally, surface properties like porosity, defects, and functional groups can enhance the accessibility of active sites and improve mass transport, further boosting $H_2O_2$ production. In addition, the electrolyte (e.g., ion tpye, pH value) also plays a critical role in tuning the reaction kinetics and selectivity. Overall, achieving high activity and selectivity in $H_2O_2$ electrocatalysis requires a balance modulation of these factors.

The electrochemical synthesis of $H_2O_2$ using carbon-based electrocatalysts involves complex reaction mechanisms that govern their performance in terms of activity, selectivity, and stability. Density functional theory (DFT) calculations (**Figure 2a**) reveal that certain defect configurations in carbon-based materials appear at the pinnacle of the $2e^-$ ORR volcano plot,[2] highlighting their role as highly active sites. Based on the fundamental mechanisms, key engineering strategies are categorized into: 1) modulation of materials'surface that governs selectivity and mass transfer, 2) reaction pathways and intermediates, and 3) selection of electrolyte. This section provides a cohesive framework for understanding the underlying principles of electrocatalysis $H_2O_2$ production (**Figure 2b**), which is crucial for optimizing the reactant adsorption/activation, stabilization of intermediates, and efficient product release.

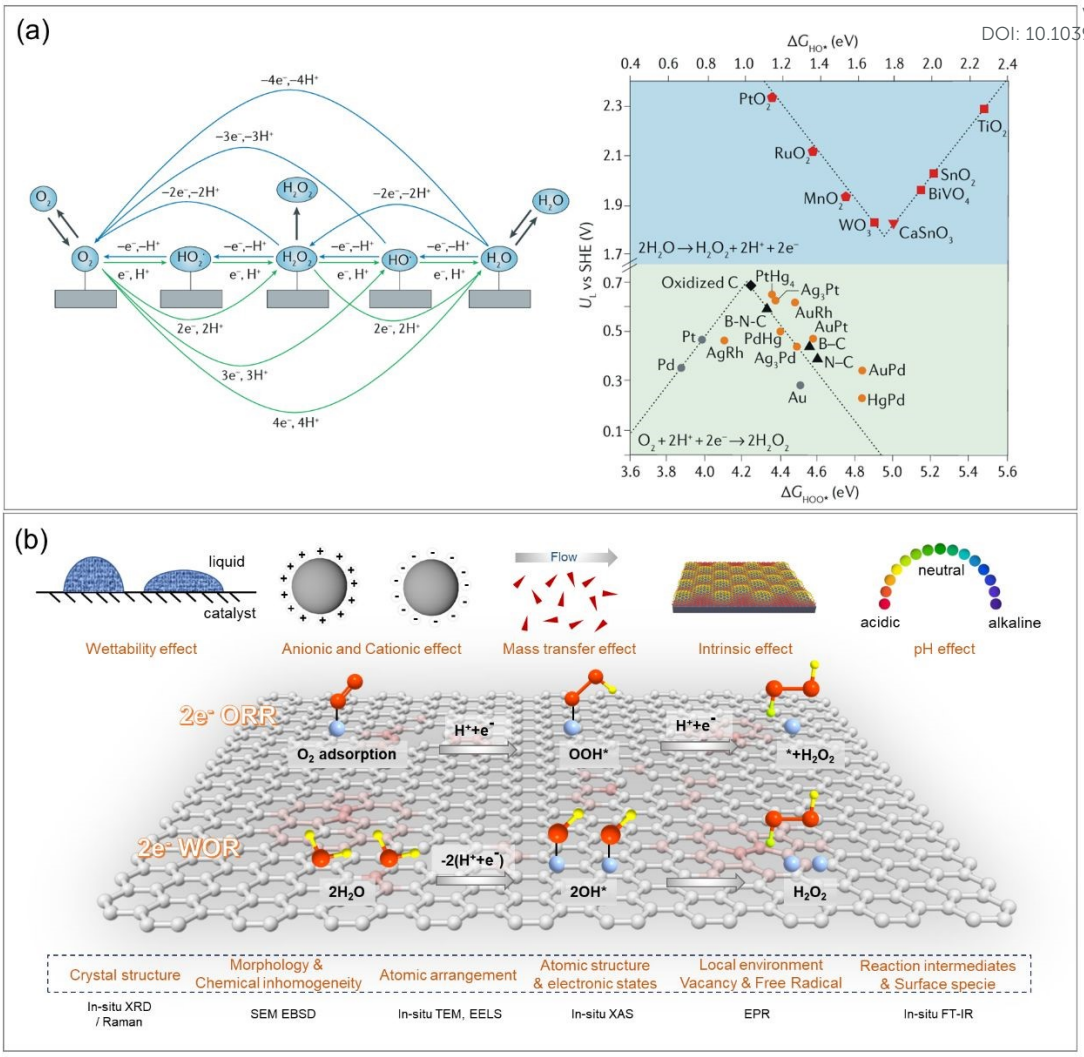


**Figure 2.** (a) Possible reduction pathways of ORR and WOR for electrocatalysis $H_2O_2$ production (left) and a plot of theoretical limiting potential ($U_L$) against Gibbs free energies of binding *OOH ($\Delta G_{HOO*}$) and *OH ($\Delta G_{HO*}$) for $H_2O_2$ electrosynthesis (right) of different types of electrocatalysts. $U_L$ is the least positive (anodic) or negative (cathodic) potential at which both electron transfers are downhill in free energy.[2] Copyright 2019, Nature Publishing Group. (b) Schematic illustration of crucial factors and characterization techniques for investigating the electrocatalytic mechanism.

### *2.3.1. Surface properties of electrocatalysts*

The surface properties of electrocatalysts, where charge and mass transfer of electrochemical reaction occurs, have crucial effect on the reaction activity.[68] The surface electronic structure of electrocatalyst directly determines the adsorption behavior of oxygen-bearing intermediates

View Article Online
DOI: 10.1039/D5MH00221D

(O*, OH*, and OOH*), thereby influencing the activity and selectivity of both the 2e⁻ ORR and WOR. For instance, defect engineering (e.g., edge sites, topological defects, curvature effects, and doping) modulates surface electronic structures and creates active sites to stabilize *OOH and activate $O_2$, leading to reduced reaction barriers and favoring the formation of $H_2O_2$. In addition, introducing single-atom catalysts on the surface of carbon materials provide precise control over adsorption and binding energies. Microstructure tailoring, such as designing mesoporous hollow nanoreactors, can enhance mass transport and intermediate retention by facilitating $O_2$ enrichment and $H_2O_2$ diffusion.

Moreover, the wettability of reaction interface, especially hydrophilicity/hydrophobicity, plays an important role in regulating the adsorption/desorption dynamics of products on electrode surface.[69] For instance, hydrophilic surfaces may facilitate ion transport and reduce gas bubbles overpotential, while controlled hydrophobicity can promote $O_2$ diffusion to active sites, a crucial factor for the ORR. The balance between hydrophilic and hydrophobic domains can be optimized through chemical functionalization or micro/nanostructuring to create ideal triple-phase boundaries for simultaneous $O_2$ supply and $H_2O_2$ release.[70-72] When combined with other catalyst modifications (defect engineering, heteroatom doping, etc.), wettability control creates synergistic effects that enhance both the kinetics and thermodynamics of the 2e⁻ pathways, bridging fundamental mechanistic understanding with practical catalyst optimization for efficient $H_2O_2$ production.

*2.3.2. Reaction pathways and intermediates*

Both the 2e⁻ ORR and WOR pathways enable selective $H_2O_2$ production, yet they proceed through fundamentally different reaction mechanisms involving critical intermediates. Theoretical studies have established that the binding energies of $\Delta G_{OOH*}$ and $\Delta G_{OH*}$ serve as main descriptors for catalysts to favour $H_2O_2$ formation from $O_2$ or $H_2O$, respectively.

Based on the ORR mechanism, three factors are crucial to ensure high $H_2O_2$ production selectivity.[73, 74] Firstly, a suitable $O_2$ adsorption model is necessary to prevent the dissociative

pathway. When the adsorption state is in Pauling mode, the O−O bond is unlikely to break, which is favorable for the generation of $H_2O_2$. Secondly, the catalysts should balance the strong adsorption of $O_2$ to facilitate OOH* generation, while allowing moderate desorption to produce $H_2O_2$ rather than $H_2O$. Thirdly, it is important to ensure rapid release of the produced $H_2O_2$ from the catalyst surface to avoid further reduction or decomposition.

As for the WOR process, the selectivity among the $1e^-$, $2e^-$, and $4e^-$ pathways is determined by the descriptors $\Delta G_{*OH}$ and $\Delta G_{*O}$, where $\Delta G_{*O} - 2\Delta G_{*OH} = 0.28$ eV.[75, 76] The selectivity of $H_2O_2$ production depends on the recombination of two *OH intermediates; If *OH is further oxidized to *O or •OH, the $H_2O_2$ formation is suppressed. At $\Delta G_{*OH} = 2.38$ eV, *OH can form either $H_2O_2$ or *O. If the adsorption energy of *O exceeds the production energy of $H_2O_2$ (3.52 eV), the reaction favors the $4e^-$ pathway (with $\Delta G_{*O} < 3.52$ eV and $\Delta G_{*OH} < 1.62$ eV). The optimal condition for the target $2e^-$ WOR occurs when $\Delta G_{*OH}$ is between 1.62 and 2.38 eV, as the standard potential is more positive than that of $H_2O_2$ oxidation ($E^0 = 0.67$ $V_{RHE}$).

*2.3.3. Role of electrolyte*

The electrolyte is also critical in electrochemical $H_2O_2$ production process, particularly when pairing $2e^-$ ORR and $2e^-$ WOR in traditional liquid electrolytes ranging from acidic to alkaline pH. For $2e^-$ ORR, the pH of electrolyte affects the selectivity due to the solvation effects and surface adsorbed species (such as $*OH_{ads}$ and anions).[22, 77] In alkaline medium, the •OH species are strongly adsorbed on the catalyst surface, facilitating outer-sphere electron transfer via water-solvated molecular $O_2$. In contrast, acidic electrolytes promote high proton mobility, resulting in low concentrations of adsorbed •OH species. Here, $O_2$ molecules are chemisorbed on the catalyst surface, receiving electrons through the inner-Helmholtz plane (IHP) process.[78]

## 3. Engineering strategies for carbon-based electrocatalysts

The catalytic performance of materials is intrinsically determined by the physicochemical properties of their surfaces, which govern the adsorption and desorption of reactive species and influence key parameters such as activity, selectivity, and stability. Pristine carbon materials

View Article Online
DOI: 10.1039/D5MH00221D





often suffer from low catalytic activity and poor selectivity due to their relatively inert surfaces and limited active sites. To overcome these inherent limitations, a range of advanced engineering strategies have been developed, including microstructure design, defect engineering, chemical doping, surface functionalization, and introduction of heterojunction or atomic sites, to enhance the electrocatalytic performance of carbon nano-catalysts toward $H_2O_2$ production, primarily focusing on the $2e^-$ ORR pathway. The roadmap of carbon-based electrocatalysts illustrating the key findings is summarized in **Figure 3**.

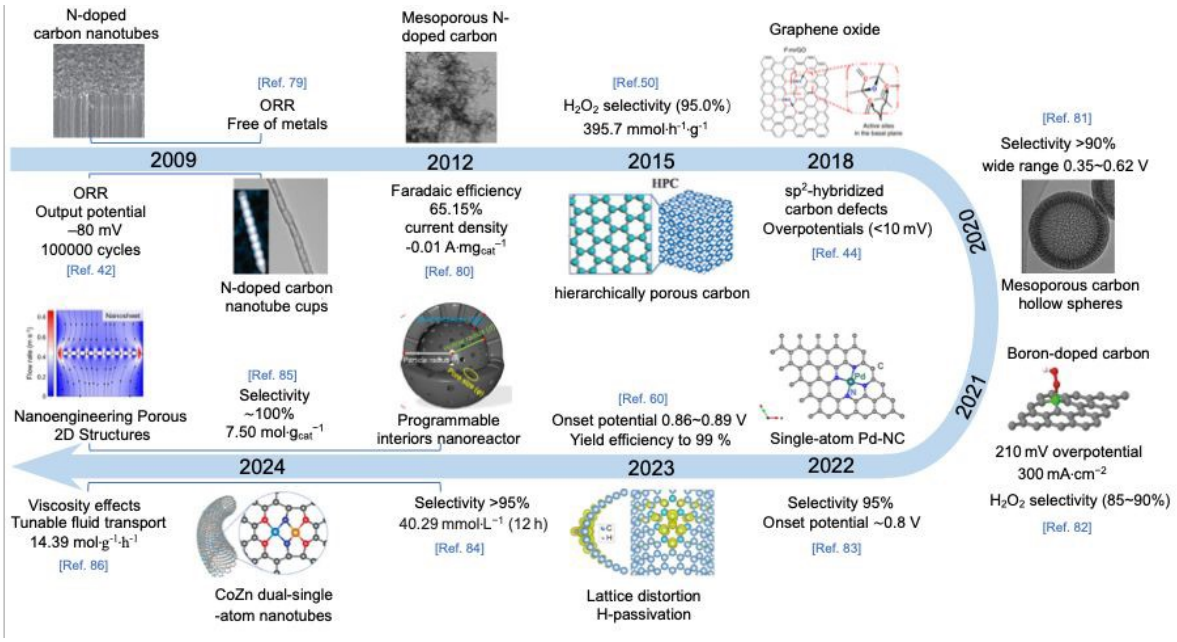


**Figure 3.** Timeline of engineering strategies for carbon-based electrocatalysts for $H_2O_2$ production: N-doped carbon nanotubes,[42] reduced graphene oxide,[44] hierarchically porous carbon,[50] N-doped carbon nanotubes cups,[79] mesoporous N-doped carbon,[80] Mesoporous carbon hollow spheres,[81] boron-doped carbon,[82] single-atom Pd/carbon,[83] Lattice distortion Carbon,[60] mesoporous carbon spheres,[84] CoZn dual-single-atom carbon nanotubes,[85] and porous 2D structures.[86]

### 3.1. Microstructure tailoring

Modifying the microstructure of carbon materials plays a vital role in boosting their catalytic performance. Constructing various nanostructures, such as 1D (e.g., nanotube and nanorods), 2D (e.g., graphene), porous architectures (e.g., macropores, mesopores and micropores), and hierarchical structures, leads to significant improvements in surface area, exposure of active

View Article Online
DOI: 10.1039/D5MH00221D

sites, mass diffusion, and electrical conductivity. These enhanced properties are crucial for increasing the efficiency and selectivity of the catalyst during the electrocatalysis process.

The catalytic performance of microstructures is heavily influenced by their dimensions and porosity, as these factors determine the accessibility of active sites and the transport of reactants and products.[87, 88] For example, 1D nanostructures such as nanotubes provide excellent electron transport pathways, while 2D nanostructures like graphene sheets offer high surface areas for active site exposure. Moreover, when porous architectures are introduced, such as macropores (larger pores that facilitate mass transport), mesopores (intermediate-sized pores that enhance exposure of active sites), and micropores (smaller pores that control the retention of reactants), the material's ability to regulate reaction intermediates and diffusion kinetics can be greatly promoted.[89] Moreover, the $2e^-$ ORR can be regulated by controllable pore structures through adjusting the coordination of reaction intermediates. By optimizing the exposure of active sites and retention time of $H_2O_2$ within specialized pore sizes, the overall performance of the catalyst can be finely tuned.[51, 90] Recently, hollow structures that typically feature lower density and larger surface area, have garnered significant attention due to their unique properties compared to solid counterparts, by facilitating mass transport and enhancing the availability of active sites. The increased surface-to-volume ratio in hollow structures further contributes to higher utilization of the catalyst material, making them highly attractive for electrocatalytic $H_2O_2$ production.[81, 91-93] This section will mainly focus on the key latest advances in the rational design of high efficient carbon-based electrocatalysts with controllable microstructures.

View Article Online
DOI: 10.1039/D5MH00221D



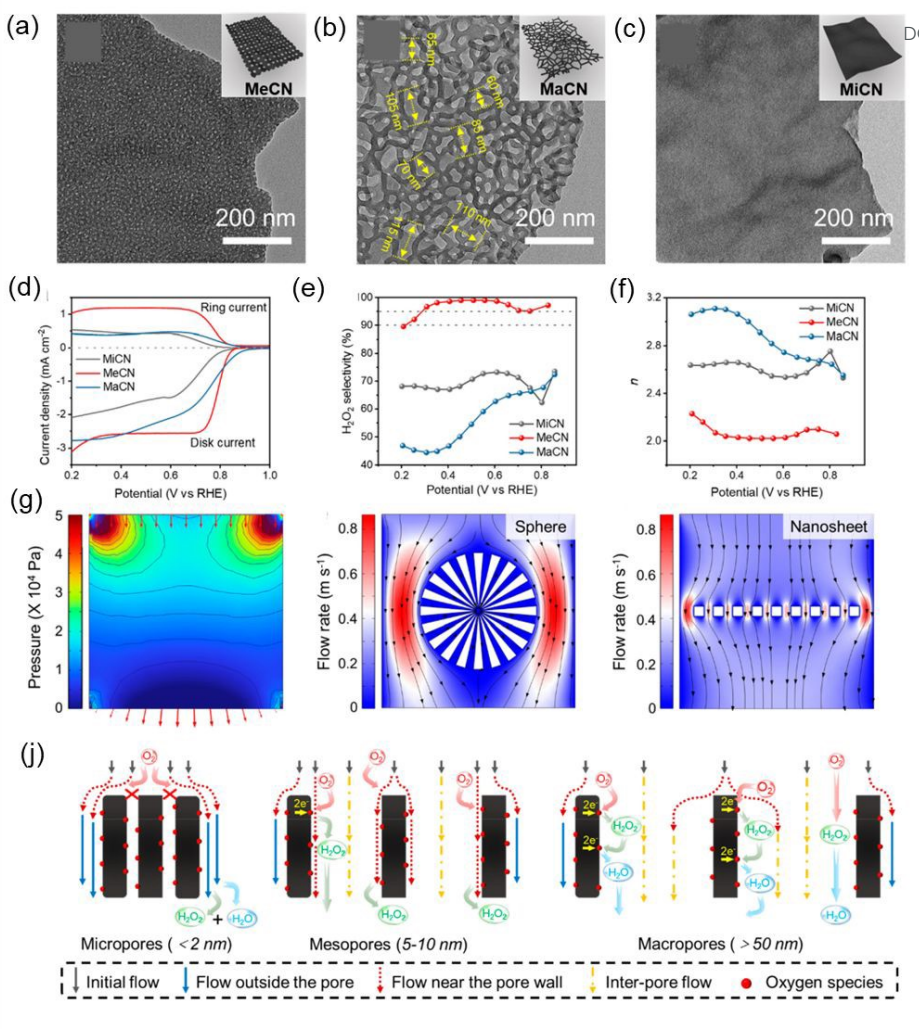


**Figure 4.** Nanoengineering of porous 2D carbon structures for ORR $H_2O_2$ production. TEM images and structural models of (a) MeCN, (b) MaCN, and (c) MiCN; (d) LSV curves recorded in an $O_2$-saturated KOH, (e) calculated $H_2O_2$ selectivity, and (f) ORR electron transfer number at various potentials; (g) Color mapping of the spatial pressure distribution, and spatial distribution of flow velocities of the mesoporous carbon sphere and nanosheet model (pore size: 5 nm); (j) Proposed fluid behavior and ORR processes in micropores, mesopores, and macropores. Reproduced with permission.[86] Copyright 2024, the American Chemical Society.

Precision nanoengineering of porous 2D structures has been emerging as a promising strategy for fine-tuning catalytic reactions. Guided by finite element simulations (FEM), Tian *et al.*[86] designed and fabricated porous 2D carbon nanomaterials by introducing mesopores with diameters of 5–10 nm to facilitate fluid acceleration (**Figure 4**a-c). The resulting mesoporous carbon nanosheets exhibited exceptional electrocatalytic $H_2O_2$ production performance, achieving a high selectivity of >95% and a diffusion-limiting disk current density of −3.1 mA $cm^{-2}$ (**Figure 4**d-f). FEM simulations revealed that the mesoporous nanosheet significantly

View Article Online
DOI: 10.1039/D5MH00221D

accelerated fluid flow within the meso-channels due to viscosity effects and the constricted flow path (**Figure 4**g), validating the crucial role of mesoporous 2D structures in enhancing local diffusion. Remarkably, the electrolysis process in a flow cell achieved a high production rate of 14390 mmol $g^{-1}$ $h^{-1}$, yielding a medical-grade $H_2O_2$ solution. This work demonstrates an effective approach to improving the activity and selectivity of porous carbon materials by influencing local fluid transport behavior.

Mesoporous hollow nanoreactors (MHNs), a novel class of rationally designed catalytic material, offer unique advantages of complex catalytic processes due to their hollow internal spaces and mesoporous structures.[94-96] The mesoporous channels can create a confined microenvironment that enhances molecular diffusion, adsorption and surface reactions, enabling tunable catalytic pathways. For instance, Tian *et al*.[84] demonstrated precisely engineered carbon spheres by integrating micromechanics with controllable synthesis to improve their $2e^-$ ORR catalytic activity (**Figure 5**). The mesoporous channels accelerated fluid flow and facilitated the transport of generated $H_2O_2$ into the solution (**Figure 5**a-c), thereby minimizing electro-reduction on the catalysts' surface. Increased flow rates led to $O_2$ enrichment in the pore channels (**Figure 5**d), while the accumulation of $OH^-$ ions (**Figure 5**e) elevated the local pH within the MHNs. And the surface of $MHCS_{0.5}$ electrode demonstrated the highest $OH^-$ concentrations among all samples (**Figure 5**f). As a result, $MHCS_{0.5}$ exhibited exceptional $2e^-$ ORR performance in neutral electrolyte conditions (pH = 7), with a diffusion-limited disk current of $-2.8$ mA $cm^{-2}$ at 0.2 V an onset potential of 0.6 V (vs. RHE), and an $H_2O_2$ selectivity exceeding 85%, outperforming most carbon-based catalysts reported in the literature.

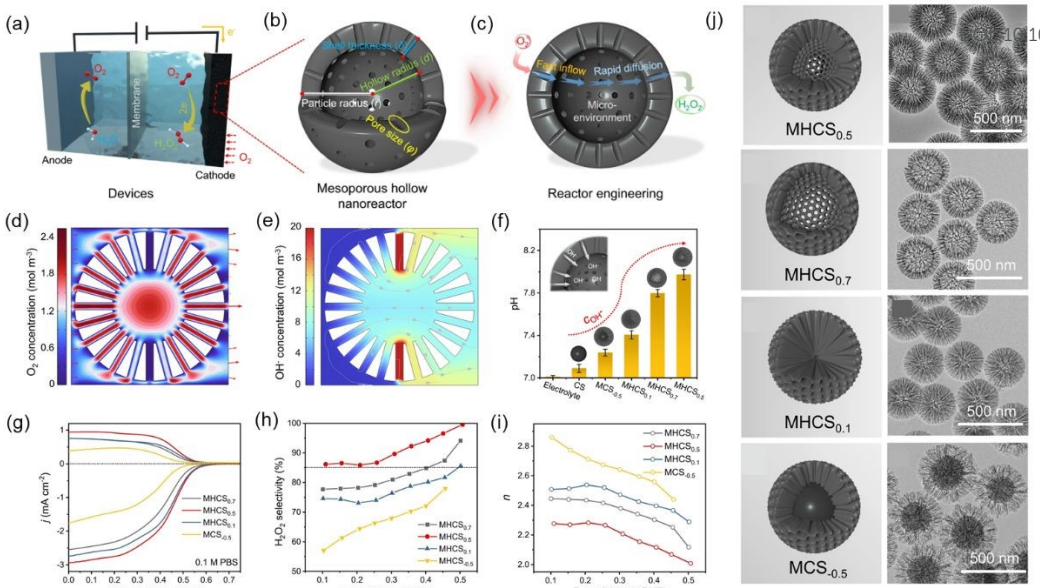


**Figure 5.** Nanoreactor design based on carbon nanospheres. (a-c) Schematic diagram for electrochemical $2e^-$ ORR to produce $H_2O_2$ over the designed nanoreactor; Spatial distribution of (d) $O_2$ and (e) $OH^-$ concentration in the mesoporous carbon sphere model; (f) $OH^-$ concentrations on the surface of $MHCS_x$; (g) LSV curves of RRDE measurements, (e) $H_2O_2$ selectivity, and (i) electron transfer number at various applied potentials; (j) Structural model and TEM images of $MHCS_x$. Reproduced with permission.[84] Copyright 2024, Nature Publishing Group.

### 3.2. Defect engineering

Defects in carbon nanomaterials, such as vacancies, rings, edge sites, topological defects, and lattice distortion, play a crucial role in modulating their electronic structure and surface chemistry. Introducing structural defects can generate abundant active sites that enhance the adsorption and activation of oxygen molecules, thereby improving the selectivity and efficiency of the ORR towards $H_2O_2$ production.[97, 98] For instance, vacancies provide more exposed active sites, while edge defects create abundant unsaturated bonds.[99] Beyond enhancing catalytic reactivity, defect engineering could also improve the durability and stability of the electrochemical system, making it more suitable for industrial applications.[97] In the past decade, significant efforts have been made to explore defective carbon catalysts for electrochemical $H_2O_2$ production.[100-104] In this section, we will highlight the key advances in defect engineering

View Article Online
DOI: 10.1039/D5MH00221D

of carbon electrocatalyst including both intrinsic defects (e.g., edge defects, topological defects) and chemical doping with heteroatoms (e.g., single element and dual-elements doping).

*3.2.1 Intrinsic defects*

Edge engineering has emerged as a promising strategy to activate inert carbon surfaces and modify their local electronic structure by introducing unpaired electrons.[105, 106] For example, Jing *et al*.[99] developed an organic-inorganic hybrid co-assembly approach to fabricate mesoporous carbon nanofibers (MCNFs) with tunable edge site densities and pore sizes, using ammonia to catalyze the modular molding of $SiO_2$ and resin (**Figure 6**a). They demonstrate that the density of carbon edge sites can be controlled to enhance ORR activity and selectivity. The optimized MCNFs catalyst exhibited outstanding $2e^-$ ORR performance (**Figure 6**b and c), achieving high $H_2O_2$ selectivity (>90%) over a wide potential range of 0.6 V, along with a large cathodic current density of −3.0 mA $cm^{-2}$ at 0.2 V vs. RHE. As illustrated in **Figure 6**d, the defect configurations comprised vacancies (VD1 and VD2), topological defects (TD3), and edge defects, including zigzag and armchair types (ZD4 and AD5, respectively). The introduction of these defects enhanced *OOH adsorption, with the zigzag defect (ZD4) and armchair (AD5) defects exhibiting free energies of 3.67 and 3.62 eV, respectively, values close to the ideal standard free energy of 3.52 eV (**Figure 6**e and f). These results demonstrate that edge defects can effectively promote the $2e^-$ ORR pathway, offering a promising route to achieving high $H_2O_2$ production activity selectivity in carbon-based electrocatalysts.

View Article Online
DOI: 10.1039/D5MH00221D



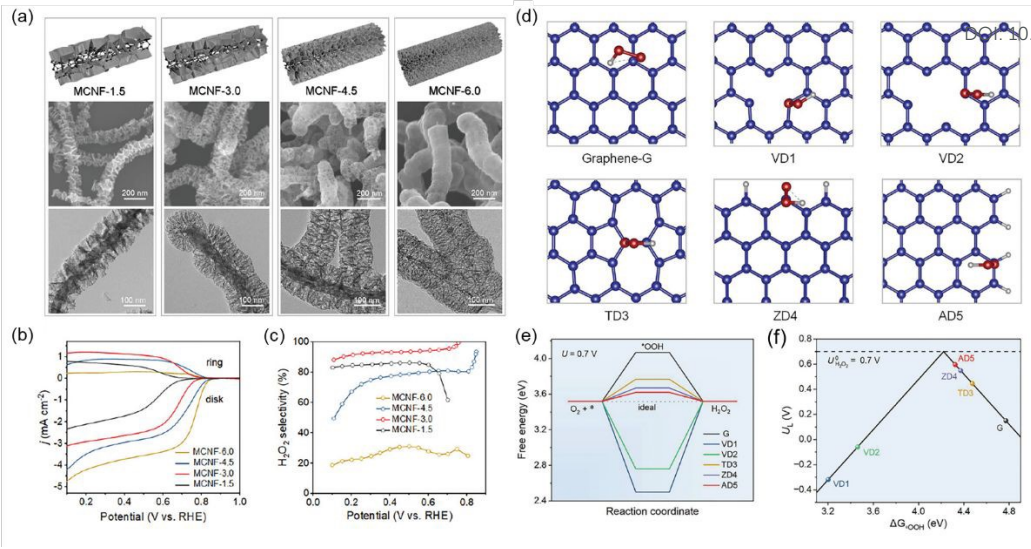


**Figure 6.** Edge defect engineering of ORR activity. (a) Schematic, SEM, and TEM images of different mesoporous carbon nanofibers (MCNFs); (b) LSV curves and (c) calculated $H_2O_2$ selectivity; (d) Preferred *OOH adsorption configurations on pristine graphene and different carbon defects models (blue, grey, and red represent C, H, and O atoms, respectively); (e) Free-energy profiles of ORR paths at potential of 0.7 V; (f) Volcano plot for the most active structures, with the limiting potential depicted as a function of $\Delta G_{*OOH}$. Reproduced with permission.[99] Copyright 2023, Wiley-VCH.

By introducing asymmetric structures into hexagonal carbon lattice, the symmetry can be broken to allow rapid electron transfer, thus promoting the electrocatalytic process. Recently, topological defects have been recognized as effective active sites toward catalyzing different electrochemical reactions. She *et al.*[107] investigated the curvature-dependent ORR activity of surface oxidized carbon nanotubes (o-CNTs) (**Figure 7**a-d). Computation modeling suggested that the curvature can alter epoxy group geometry, exerting greater strain on the C–O bond in smaller diameter o-CNTs that leads to improved activity. Increase of *R* results in stronger OOH* binding and a lower $\Delta G_{OOH*}$ (**Figure 7**c), and 2e-ORR theoretical potential ($U_L$) approaches the equilibrium potential ($E^0$ = 0.69 V) on a model with a greater *R* (**Figure 7**d). As predicted, the o-CNT with the smallest diameter (~8 nm) exhibited the highest Faradaic efficiency >85% and a mass activity of 161 A $g^{-1}$ at 0.65 V. Very recently, Wang *et al.*[108] fabricated carbon nanomaterials with rich topological defect sites and curved defective surface by controlling the pyrolytic shrinkage process of precursors (**Figure 7**e-i). Theoretical

calculations demonstrated that bending the defect sites can manipulate the local electronic structure, facilitate the charge transfer to key intermediates, and reduce the ORR energy barrier. Experimental results showed that a large kinetic current density of 22.5 mA $cm^{-2}$ at 0.8 V vs. RHE was obtained for high-curvature defective carbon (HCDC), which is ~18 times of low-curvature defective carbon (LCDC). Further increasing the defect densities of HCDC results in a dual-regulated product (HCHDC), which exhibited exceptional ORR activity in both alkaline and acidic media (half-wave potentials of 0.88 and 0.74 V, respectively), exceeding most of the reported carbon electrocatalysts. These studies highlight the crucial role of curvature effect in promoting electrocatalytic activity and offer new guidance to the design of advanced carbon nano-catalysts for $H_2O_2$ production.

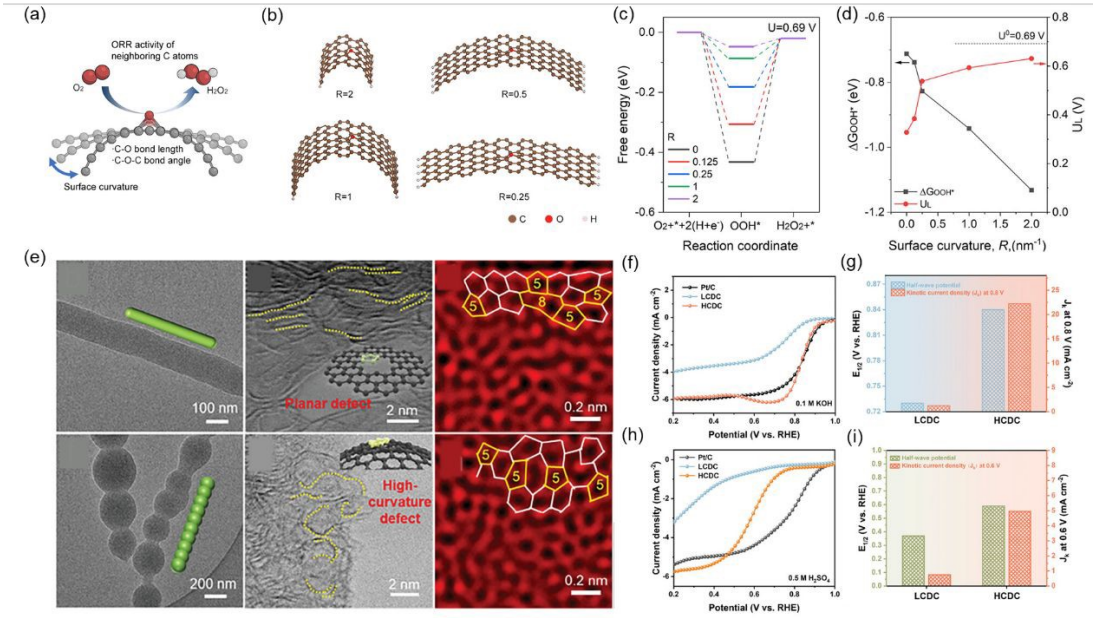


**Figure 7.** Investigation of the curvature-dependent ORR activity. (a) Schematic illustration of the epoxy group grafted on curvature varied carbon surface and (b) geometry optimized atomic models of different *R* values; (c) Calculated ORR free energy diagrams at 0.69 V and (d) correlations between $\Delta G_{OOH*}$ and $U_L$ to surface curvature. Reproduced with permission.[107] Copyright 2024, the American Chemical Society. (e) TEM, HRTRM, and AC HAADF-STEM images of LCDC and HCDC (insets are morphology and atomic structure diagrams); (f) LSV curves in $O_2$-saturated KOH and (g) comparison of $J_k$ (0.8 V) and $E_{1/2}$; (h) LSV curves of LCDC, HCDC, and Pt/C in $O_2$-saturated $H_2SO_4$ and (i) comparison of $J_k$ (0.6 V) and $E_{1/2}$. Reproduced with permission.[108] Copyright 2024, Wiley-VCH.

*3.2.2 Heteroatom doping*

Incorporating non-metallic/metallic heteroatoms, such as boron (B),[109-111] nitrogen (N),[103, 112] oxygen (O),[113, 114] fluorine (F),[113] and sulfur (S),[115] into the carbon lattice can disturb the electron symmetry in the aromatic carbon networks, providing the inhomogeneous compositions and active sites by means of tailoring the charge and spin densities of carbon atoms. In addition, heteroatoms could introduce active functional groups (oxygen-bearing functional groups) onto the carbon matrix, which can serve as active sites for $2e^-$ ORR, to achieve high electrocatalysis activity. Up till now, extensive studies have been reported on this strategy, herein we only summarize the latest achievements on heteroatom doping to enhance electrocatalytic $H_2O_2$ generation activity.

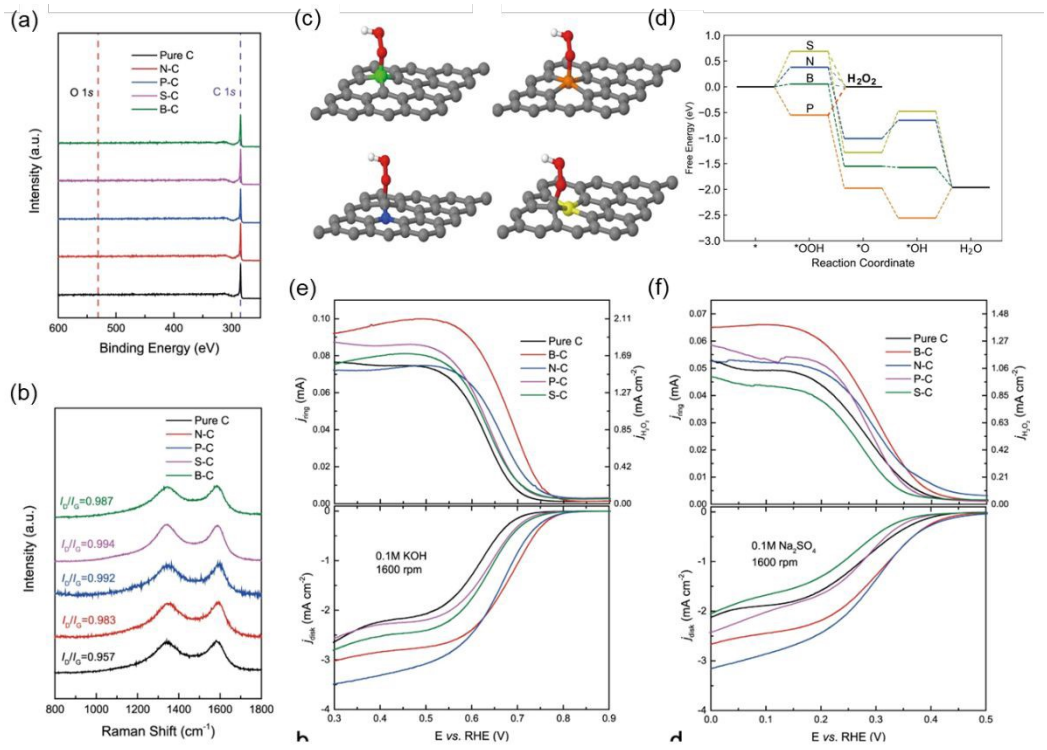


**Figure 8.** Heteroatom-doped carbon catalysts for electrocatalytic $H_2O_2$ generation. (a) XPS survey scan and (b) Raman spectroscopy for pure C and B, N, P, S-doped carbon catalysts; (c) Preferred *OOH adsorption configurations on B-, P-, N-, and S-doped graphene, respectively. Green, orange, blue, yellow, gray, red, and white spheres represent B, P, N, S, C, O and H, respectively; (d) Free-energy profile of $O_2$ reduction paths ($U_{RHE} = 0.7$ V); LSV curves and $H_2O_2$ currents (1.2 V vs. RHE) recorded by RRDE in (e) 0.1M KOH and (f) 0.1M $Na_2SO_4$. Reproduced with permission.[82] Copyright 2021, Nature Publishing Group.

In 2021, Xia *et al.*[82] reported a boron-doped carbon (B-C) catalyst (**Figure 8**). Compared to the state-of-the-art oxidized carbon catalyst, the B-C catalyst presented significantly lowered overpotential by 210 mV under industrial-level currents (300 mA $cm^{-2}$) while maintaining high $H_2O_2$ selectivity (85–90%) (**Figure 8**e and f). DFT calculations revealed that the boron dopant site is responsible for high $H_2O_2$ activity and selectivity due to the reduced thermodynamic and kinetic reaction barriers (**Figure 8**c and d). Integrated in a porous solid electrolyte reactor, the B-C catalyst demonstrated continuous generation of pure $H_2O_2$ solutions with high a current density (~400 mA $cm^{-2}$) and selectivity (~95%), presenting their great potential for practical applications in the future.

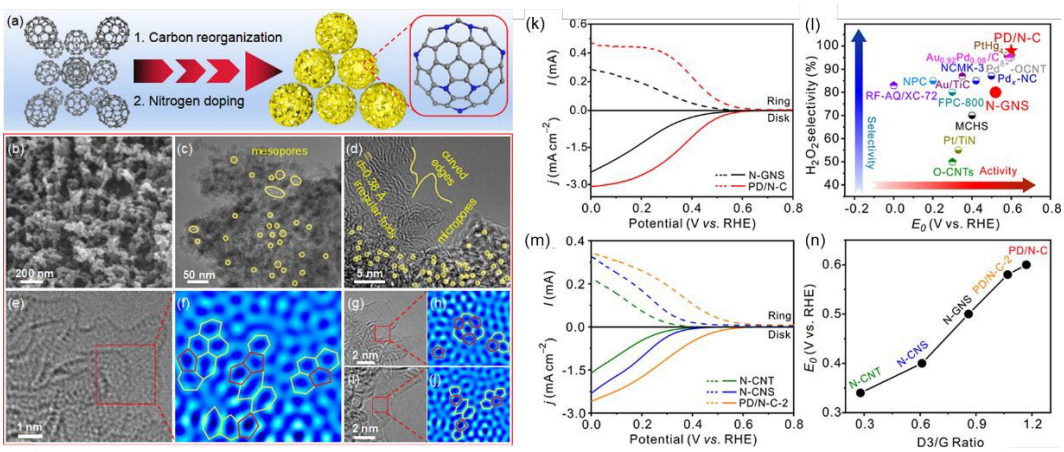


**Figure 9.** Pentagonal defect-rich N-doped carbon nanomaterial (PD/N–C) using fullerene ($C_{60}$). (a) Schematic of the synthesis of PD/N–C; (b) SEM, (c,d) TEM, and (e,g,i) AC-STEM images and (f,h,j) the corresponding Fourier transform fitting results of PD/N–C; (k) RRDE polarization curves and $H_2O_2$ currents at the ring electrode of PD/N–C and N-GNS; (l) Comparison of $2e^-$ ORR performance of representative electrocatalysts; (m) RRDE polarization curves and $H_2O_2$ currents at the ring electrode of N-CNT, N-CNS, and PD/N–C-2; (n) Onset potential ($E_0$) as a function of the D3/G ratio of a series of samples. Reproduced with permission.[103] Copyright 2023, the American Chemical Society.

Oxygen-doped carbon quantum dots (o-CQD) with C–O–C surface functional groups was fabricated with tunable electronic structure by varying isomerization precursors,[114] presenting a remarkable $H_2O_2$ selectivity of 96.2% ($n$ = 2.07) at 0.68 V vs. RHE along with a low Tafel slope of 66.95 mV $dec^{-1}$, and maintaining consistent production stability of $H_2O_2$ over 120 h. In addition, hierarchical porous boron-doped carbon (B-DC) electrocatalyst was synthesized

View Article Online
DOI: 10.1039/D5MH00221D

from fullerene ($C_{60}$) frameworks and boric oxide.[109] Befitting from boron doping and abundant topological pentagon defects, the B-DC catalysts exhibited a high ORR onset potential of 0.78 V and a $2e^-$ selectivity over 95%. Remarkably, the B-DC electrocatalyst-based device achieved a remarkable $H_2O_2$ yield rate of 247 $mg \cdot L^{-1} \cdot h^{-1}$ and quantitative Faraday efficiency of nearly 100%. For sulfur-doped defective nanocarbons (S-DNC), a similar high ORR onset potential (0.78 V) and selectivity (90%) was obtained, with an superior $H_2O_2$ yield rate of 690 mg $L^{-1}$ $h^{-1}$ in a H cell.[115] In 2023, Lu *et al*.[103] designed and fabricated a pentagonal defect-rich N-doped carbon nanomaterial (PD/N–C) via pyrolysis of $C_{60}$ as the precursor followed by ammonia treatment (**Figure 9**a). A great number of mesopores and micropores were created in PD/N–C, along with abundant irregular folds and curved edges (**Figure 9**b–d). Moreover, the aberration-corrected scanning TEM (AC-STEM) and the corresponding fitting results (**Figure 9**e–j) further demonstrate that the PD/N–C sample contains rich pentagon defects. As a result, the PD/N−C catalysts achieved excellent $2e^-$ ORR activity, selectivity, and stability in acidic electrolytes, even outperforming the Pt-Hg alloy catalyst. The linear sweep voltammetry curves (**Figure 9**k) show that the PD/N–C catalyst achieves a larger ORR current density (3.1 mA $cm^{-2}$ at 0 V) along with a higher onset potential in a wide potential range from 0 to 0.6 V, as compared to N-doped carbon nanomaterial dominated by hexagons graphene nanosheets (N-GNS). This performance is among the top of all reported metal-free carbon-based catalysts and even superior to some noble-metal-based catalysts and the benchmark $PtHg_4$ alloy catalyst in acidic electrolytes (**Figure 9**l). By comparing a series of samples, the synergetic effects of both topological defects and N-doping are responsible for the superb $2e^-$ ORR performance of the PD/N–C catalysts (**Figure 9**m and n).

View Article Online
DOI: 10.1039/D5MH00221D



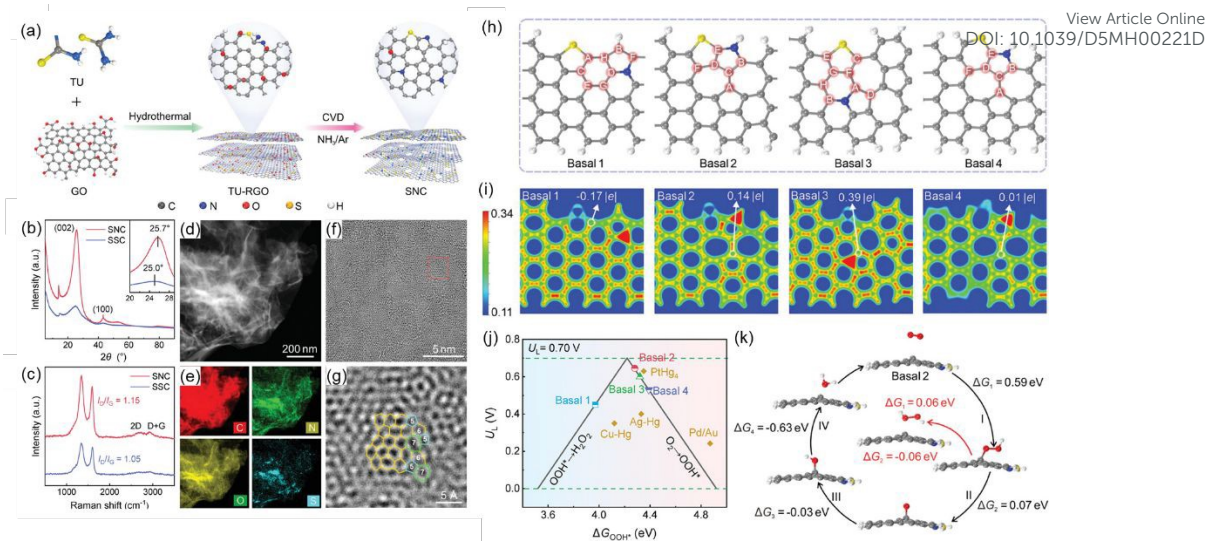


439

440 **Figure 10.** Pentagon-S and pyrrolic-N coordinated (SNC) graphene with in-plane topological
441 defects. (a) Schematic illustration of synthesis for graphene pentagon-S and pyrrolic-N
442 coordinated (SNC); (b-g) XRD patterns, Raman spectra, TEM images, and EDS mappings; (h)
443 Computational models, (i) Bader charge, (j) activity-volcano plot ($U_L$ = 0.70 V), and (k) ORR
444 reaction pathway diagrams and corresponding energy barriers for each step on Basal 2.
445 Reproduced with permission.[100] Copyright 2024, Wiley-VCH.
446
447 In addition to single-element doping, dual elements co-doping on carbon materials have been
448 received increasing research attention toward electrocatalytic 2e⁻ ORR due to the unique
449 synergistic effect.[116] For instance, a yolk-shell B/N co-doped hollow carbon nanosphere, with
450 oxygen-vacancy decorated reduced graphene oxide coating (B/N-HCNS@VO-G) was reported
451 as an efficient metal-free electrocatalyst for 2e⁻ ORR with high durability.[117] Such a dual-
452 doping electrocatalyst leads to excellent electrocatalytic $H_2O_2$ production performance with a
453 high selectivity of 91% and yield of 56 ppm (0.7 V), allowing in-situ antibiotic and dye
454 degradation for on-site wastewater remediation. Very recently, pentagon-S and pyrrolic-N
455 coordinated (SNC) graphene with in-plane topological defects was synthesized through a two-
456 step hydrothermal and nitridation procedure (**Figure 10**).[100] The SNC is composed of stained
457 hexagons with sporadic pentagons (**Figure 10**d-g), suggesting that the hexagonal topological
458 structure of the carbon matrix is significantly distorted. In addition, the dual-doping of S and N
459 elements introduces unsymmetrical dumbbell-like S–C–N motifs, which can effectively tune
460 the electronic structures of graphene (**Figure 10**h and i). Theoretical calculations further

View Article Online
DOI: 10.1039/D5MH00221D

unveiled that the defective S–C–N motifs can effectively optimize the binding strength to OOH* intermediate and reduce the energy barrier for ORR to $H_2O_2$ (**Figure 10**j). As a result, the SNC catalyst exhibited ultrahigh $H_2O_2$ production rate of 8100, 7300, and 3900 mmol $g^{-1}$ $h^{-1}$ in alkaline, neutral, and acidic electrolytes, respectively.

It is worth mentioning that doping with heteroatoms into carbon matrix could also induce surface functional groups. For example, oxygen functionalization onto the parent carbon structures has been reported to be effective to improve $2e^-$ ORR performance.[21, 118, 119] For instance, oxygen-doped carbon dots (O-CDs) was synthesized by solvent engineering approach and exhibited excellent catalytic activity.[120] By tuning the ratio of ethanol and acetone solvents during the synthesis, the surface electronic structure of the resulting O-CDs can be precisely modulated. The selectivity and activity of the O-CDs was strongly dependent on the amount of edge active C−O groups, achieving the highest $H_2O_2$ selectivity up to ~96.6% ($n$ = 2.06, 0.65 V vs. RHE) and an ultralow Tafel plot of 64.8 mV $dec^{-1}$.

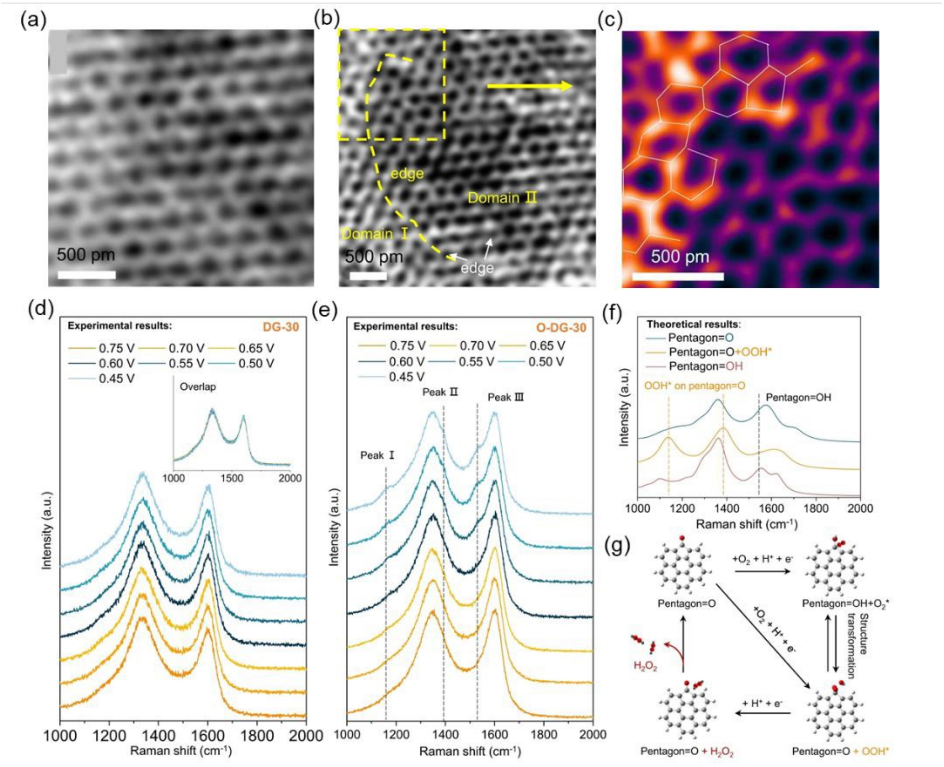


**Figure 11.** In-situ investigation of dynamic active site in oxygen modified defective graphene (O-DG) electrocatalysts. iDPC-STEM image of O-DG-30 in (a) perfect domain and (b and c)

View Article Online
DOI: 10.1039/D5MH00221D

defective domain; In-situ Raman spectra of (d) DG-30 and (e) O-DG-30 on flow cell in $O_2$-saturated 0.1 M KOH; (f) The calculated Raman spectra of three possible atomic structures of the O-groups and relevant surface species on defective graphene; (g) Schematic diagram of possible electrocatalytic mechanism of O-DG. Reproduced with permission.[121] Copyright 2023, Nature Publishing Group.

Despite tremendous works on doped carbon materials for electrocatalysis $H_2O_2$ production, the dynamic structural transformation of these materials during electrocatalysis reaction process has been received less attention. Active sites identification in carbon materials is crucial for understanding the mechanism, but resolving precise configuration of active site remains a huge challenge. In 2023, Wu *et al.*[121] manipulated the defect density and oxygen groups on graphene, and revealed the oxygen groups redistribution and positive correlation relationship between the defect density and their ORR performance (**Figure 11**). The dynamic evolution processes of defects were monitored through in-situ Raman, FTIR and XPS technologies, combined with theoretical simulations. The results clarified the configuration of major active sites (carbonyl on pentagon defect) and key intermediates (*OOH), providing deep understanding of the catalytic mechanism for doped defective carbon materials.

## 3.3. Hybrid Systems

### *3.3.1 Carbon-semiconductor heterostructures*

Recently, several studies have been reported on the coupling of carbon-based materials with metal oxides or nitrides to boost their $2e^-$ ORR activity.[122-128] Generally, the structural modulation of the carbon-metal oxide nanocomposites can rapidly release *OOH generated by the metal oxides with high activity. For instance, Qu *et al.*[122] reported the integration of CNTs with g-$C_3N_4$ to improve both electrocatalytic activity and selectivity of CNT for $H_2O_2$ production by forming a π–π interaction at their interface. The optimal g-$C_3N_4$/CNT nanocomposite catalyst exhibited almost unity (~97%) for $H_2O_2$ production at 0.50 V vs. RHE with a 2 times current density of the pristine g-$C_3N_4$ or CNT. The enhanced activity can be attributed to a synergistic effect, by which g-$C_3N_4$ provides active sites to activate $O_2$ while

View Article Online
DOI: 10.1039/D5MH00221D

CNT offers channels to facilitate electron transfer. In addition, Guo *et al.*[129] designed and prepared a novel $MnO_x$@Carbon hybrid electrocatalyst by calcinating polymer-manganese-metal-organic framework (polyMn-MOF) as the precursor under $N_2$ atmosphere. DFT calculation revealed that the optimized $MnO_x$@Carbon sample exhibited optimized adsorption energy of *OOH, with a high $H_2O_2$ selectivity of 96.5 % and large ORR current of 2.3 mA $cm^{-2}$.

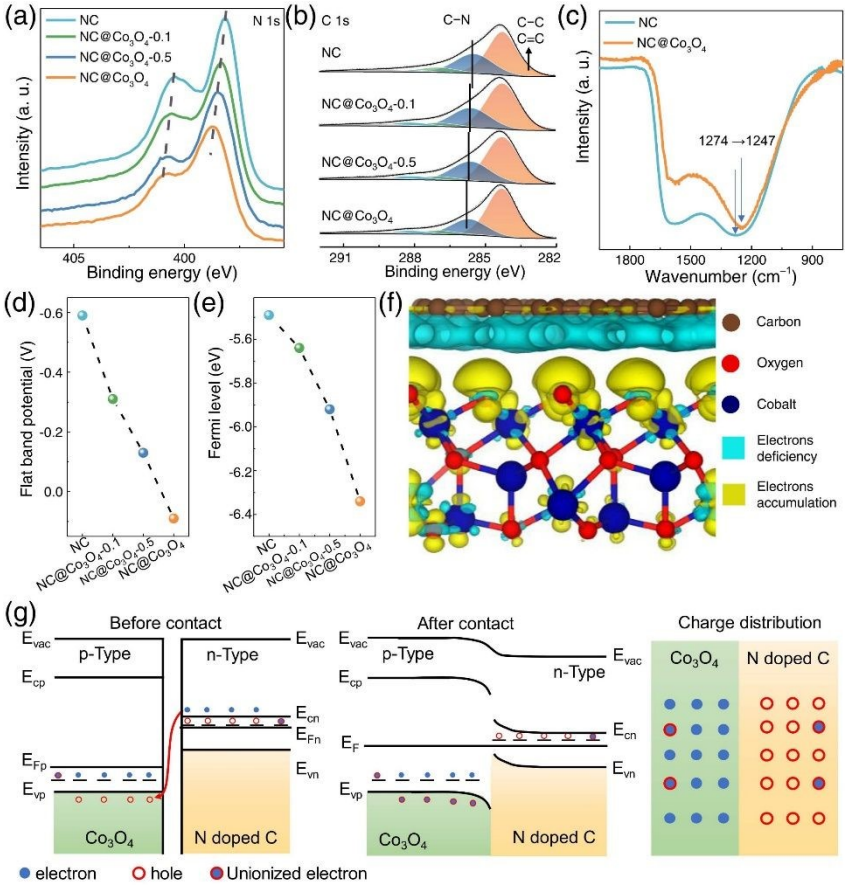


**Figure 12.** N-doped carbon and $Co_3O_4$ ($NC@Co_3O_4$) p-n heterojunction nanocomposite for electrocatalytic $H_2O_2$ production. XPS spectra of (a) N 1s and (b) C 1s; (c) FTIR spectra of NC and $NC@Co_3O_4$; (d) The flat band potential ($E_{fb}$) estimated from Mott-Schottky plots; (e) Fermi level measured by UPS; (f) Differential charge density of $NC@Co_3O_4$ heterojunction; (g) Schematic illustration of energy band and electron transfer of $NC@Co_3O_4$ p-n heterojunction. Reproduced with permission.[123] Copyright 2024, Elsevier.

Recently, Xue *et al.*[123] reported a novel p-n heterojunction nanocomposite consisting of N-doped carbon and $Co_3O_4$ ($NC@Co_3O_4$), for efficient electrocatalytic $H_2O_2$ production (**Figure 12**). Increasing Co content results in a more positive flat band potential ($E_{fb}$), indicating a decrease of the Fermi level. In addition, the differential charge density calculation demonstrated

View Article Online
DOI: 10.1039/D5MH00221D

that the electrons of the NC are transferred to the $Co_3O_4$ and promotes the affinity of O atom of $H_2O_2$ at the electron deficient carbon sites in NC, which facilitates the cleavage of O−O bonds. Consequently, the •OH generation rate catalyzed by NC@$Co_3O_4$ was 6.5 times of that by bare NC. This work highlights the promising potential of constructing carbon/semiconductor nanocomposite toward efficient $H_2O_2$ generation.

*3.3.2 Atomic-site engineered carbon hybrids*

Coordination of atomically dispersed transition metals single-atom catalysts (SACs) in a carbon matrix have proven to be effective as ORR electrocatalysts, featuring a nearly 100% utilization of metal atoms as active sites and excellent catalytic activity.[130, 131] The electronic structure of the SACs can be regulated benefiting from the strong interaction between metal atoms and the substrate, and further modulates the adsorption energy of the catalyst for oxygen-containing intermediates, which affects the $2e^-$ ORR selectivity.[132-137] As such, different SACs such as Co-SACs,[136, 138-141] Zn-SACs,[133] Fe-SACs,[142] Mn-SACs,[143] W-SACs,[144] Pt-SACs,[145, 146] Pd-SACs,[83, 92] Pb-SACs,[147] Sn-SACs [148] and In-SACs[149] have displayed superior $2e^-$ ORR performances for $H_2O_2$ production, showing large mass activity, low overpotential, and high selectivity. In this part, we emphasis the most important achievements in this field by presenting and discussing both experimental and theoretical investigations, especially the most recent advancements on more complex systems using dual-single atom carbon catalysts or coupled with other synergistic effects.

View Article Online
DOI: 10.1039/D5MH00221D



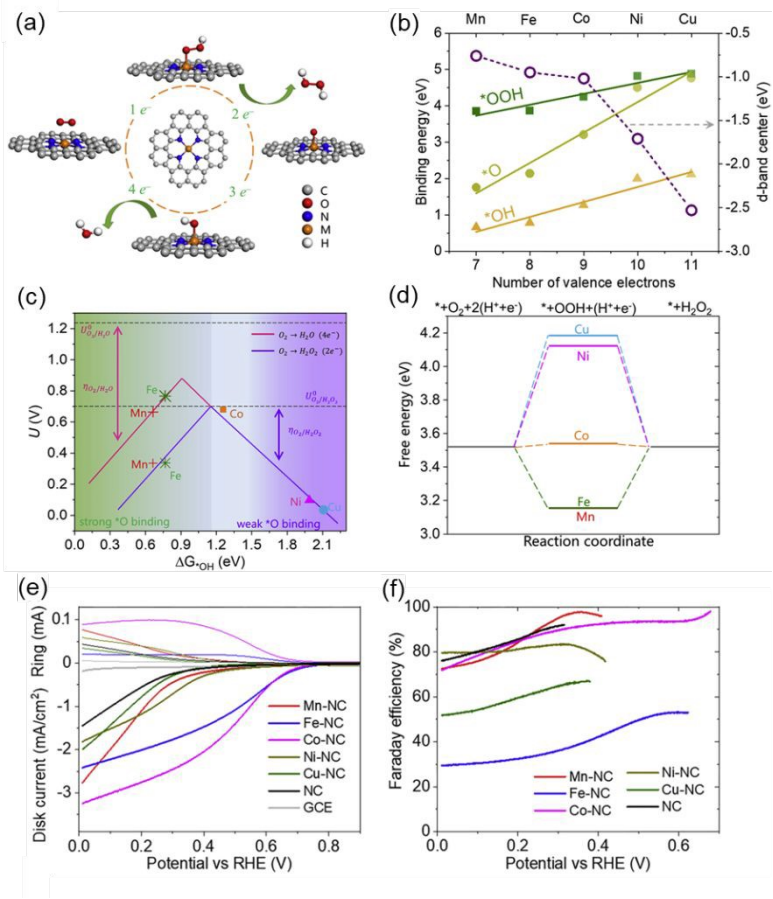


**Figure 13.** Transition metal SACs (M-SAC) (M = Mn, Fe, Co, Ni, and Cu) anchored in N-doped graphene electrocatalysts for producing $H_2O_2$. (a) Schematic of ORR; (b) Binding energy of *OOH, *O, and *OH on M-SAC and *d*-bond center of different M atoms in M-SAC; (c) Volcano curves of ORR via the $2e^-$ and $4e^-$ pathway; (d) Free energy diagrams of $2e^-$ ORR on different M-SACs (0.7 V versus RHE); (e) LSV curves and (f) Faradic efficiency as a function of potential. Reproduced with permission.[150] Copyright 2020, Cell Press.

Gao *et al.*[150] fabricated transition metal (Mn, Fe, Co, Ni, and Cu) SACs anchored N-doped graphene and systematically investigated their electrocatalytic performance for synthesizing $H_2O_2$ via ORR (**Figure 13**a). Theoretically simulations demonstrated that the Co-SAC possesses optimal *d*-band center, activity-volcano plot, and adsorption energy of the *OOH intermediate among all M- SAC samples (**Figure 13**b-d). As a result, the kinetic current for $H_2O_2$ production using Co SAC catalyst can reach up to ~1 mA $cm^{-2}$ (0.6 V vs. RHE in 0.1 M $HClO_4$) with faraday efficiency over 90% (**Figure 13**e and f), which even outperforms state-of-the-art noble-metal-based electrocatalysts in acidic media. Moreover, kinetic and in-situ X-

ray absorption analysis demonstrated that the N-coordinated single Co single-atom function as the active site for the reaction, which is rate-limited by the first electron transfer step.

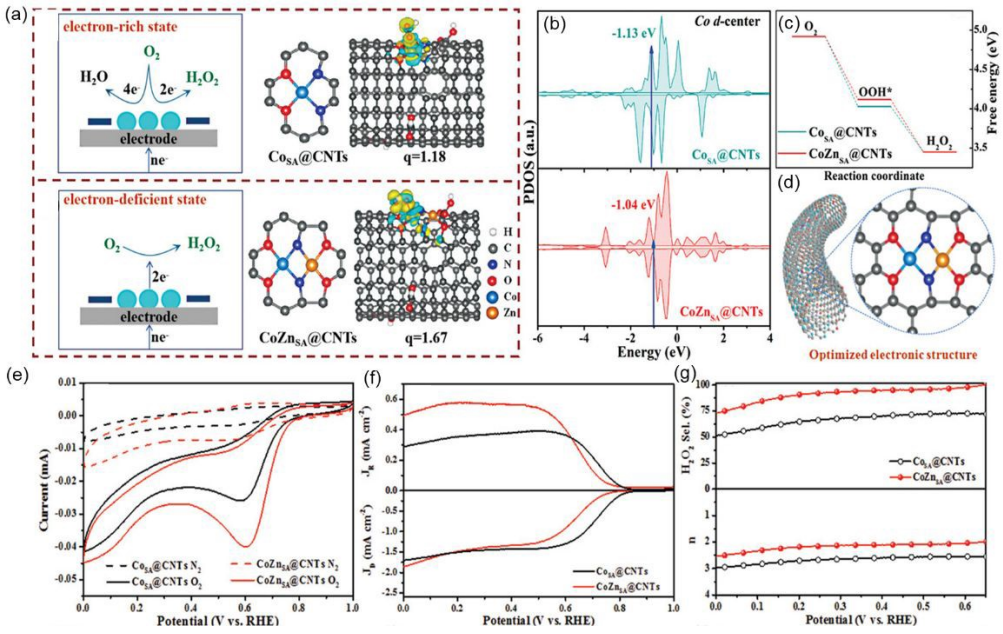


**Figure 14.** (a) Illustration of the model and their differential partial charge densities with OOH* adsorption (side view); (b) PDOS of Co 3*d* orbital and (c) Gibbs free energy diagrams of two-electron ORR of $Co_{SA}$@CNTs and $CoZn_{SA}$@CNTs, respectively; (d) Schematic of optimized electronic structure; Electrochemical performance of $CoZn_{SA}$@CNTs and $Co_{SA}$@CNTs: (e) CV curves, (b) LSV curves based on RRDE, and (g) $H_2O_2$ selectivity and electron transfer number (*n*). Reproduced with permission.[85] Copyright 2024, Wiley-VCH.

Compared to well-studied SACs, dual-atom catalysts (DACs) have received considerable attention due to the synergistic interactions between two adjacent metal sites, leading to remarkably enhanced activity, selectivity, and stability. The dual sites facilitate multi-step reactions and improve binding energies for reactants and products. In addition, DACs are more resistant to aggregation and can offer tunable properties through metal pair selection, making them ideal for complex catalytic processes. Recent advancements in DAC design have demonstrated their superior electrocatalytic performance for $H_2O_2$ production through the $2e^-$ ORR pathway.

In-N-C DACs was proposed by Du *et al.*[151] as an effective $2e^-$ ORR catalyst for producing $H_2O_2$ in acid media. The DFT calculations indicate that the valance electron number and the *d*-

View Article Online
DOI: 10.1039/D5MH00221D

band center of Co 3*d* orbital can be modulated by OH-blocked In, which leads to moderate adsorption of OOH intermediate on neighboring Co and favors 2e⁻ ORR kinetics of Co/In-N-C DACs. As a result, a partial current density of 1.92 mA $cm^{-2}$ (0.65 V in the RRDE test) was obtained, with a $H_2O_2$ production rate as high as 9680 mmol $g^{-1}$ $h^{-1}$ in a three-phase flow cell. Very recently, Yang *et al*.[85] fabricated heteronuclear CoZn DACs confined in N,O-doped hollow carbon nanotube reactors ($CoZn_{SA}$@CNTs) (**Figure 14**). The differential partial charge density calculation demonstrated that the dual-atom centers in $CoZn_{SA}$@CNTs possess more charges than that of $Co_{SA}$@CNTs (**Figure 14**a), indicating a rearrangement of the local charge distribution to facilitate the adsorption of OOH* after introducing Zn. The decrease of the *d*-band center in $CoZn_{SA}$@CNTs resulted in the appropriate adsorption of OOH* for $H_2O_2$ generation (**Figure 14**b), while inhibited the breakage of O–O bond to produce $H_2O$, ultimately facilitating the 2e⁻ ORR. In addition, $CoZn_{SA}$@CNTs model exhibited a more favorable $\Delta G_{OOH*}$ than that of $Co_{SA}$@CNTs (**Figure 14**c and d). The well-designed $CoZn_{SA}$@CNTs nanocomposite displayed outstanding electrocatalytic reactivity/selectivity for generating $H_2O_2$ in the whole pH range (**Figure 14**e-g), with a higher 2e⁻ ORR selectivity for $H_2O_2$ production than $Co_{SA}$@CNTs and $Zn_{SA}$@CNTs. In a H-type cell, $CoZn_{SA}$@CNTs/carbon fiber felt reached nearly 100% $H_2O_2$ selectivity in a range of 0.2–0.65 V (vs. RHE) with a yield rate of 1500 mmol $g^{-1}$ $h^{-1}$, surpassing most of the reported SACs. These studies highlight the great advantages of using DACs/carbon for highly efficient and selective $H_2O_2$ production.

### 3.4. Synergistic integration of multiple effects

The integrating of differnt effects, such as mophological control, engineering, and single-atom site design, creats a synergistic interplay that elevates catalytic performance beyond the simple sum of individual components. The coupling effect simultaneously enhances mass transport efficiency, electronic structure modulation, and atomic-level active site utilization, collectively optimizing the reaction pathways and maximizing overall catalytic efficiency.

View Article Online
DOI: 10.1039/D5MH00221D

Below, we discuss key coupling strategies to date, providing insights to guide future advancements in rational design of carbon-based electrocatalysts.

*3.4.1 Coupling defect/surface group with microsctructure*

Carbon materials with diverse porous structures have been reported, with simoulteneously introduction of surface functional groups. For instance, Albashir *et al*.[152] fabricated mesoporous material (Meso-PC) functionized with ketonic carbonyl (−C = O) group, which exhibites outstanding 2e⁻ ORR selectivity (~100%) at the potential of 0.4 $V_{RHE}$. This can be attributed to its precisely tailored pore structure, which facilitates the mass transfer of reactants and products. Furthermore, studies suggest that the −C = O group serve as the primary active site for 2e⁻ ORR, while a moderate surface concentration of oxygen functionalities is crucial to enchancing electrochemical $H_2O_2$ synthesis activity.

In addition, Jing *et al*.[90] demonstrated that N,O co-doped carbon nanosheets (N,O-CNS) with a hierarchical micro/mesoporous structure can create an oxygen-rich, locally alkaline-like microenvironment, significantly promoting the 2e⁻ ORR pathway in a neutral medium. Their study revealed that the hierarchical architecture not only elevates the local pH near the active sites but also facilitates the formation of intermediates ($*O_2$ and *OOH), thereby enhancing $H_2O_2$ selectivity and yield. Remarkably, the optimized N,O-$CNS_{0.5}$ catalyst achieved an exceptional $H_2O_2$ production rate of 6705 mmol $g^{-1}$ $h^{-1}$ in a flow cell, , setting a new benchmark for neutral-media electrocatalysis. This work highlights the critical role of synergistic microenvironment engineering, which combines pore structure control, heteroatom doping, and local pH modulation, in designing high-performance electrocatalysts for sustainable $H_2O_2$ synthesis.

*3.4.2 Coupling atomic active sites with microstructures*

Coupling SACs with other tailoring strategies such as microstructure modulation of carbon materials can lead to novel synergistic effects to further boost the electrocatalytic performance. As a notable example, atomically dispersed Co/Mo sites anchored on mesoporous carbon

View Article Online
DOI: 10.1039/D5MH00221D



hollow spheres (Co/Mo-MCHS) via a template-engaged strategy for highly selective ORR to $H_2O_2$ in acid.[153] Benefitting from the electron-donating effect of Mo atoms, an enriched electron density around the Co center for Co/Mo-MCHS is observed, resulting in optimal adsorption of the key $^*$OOH intermediates to approach the apex of $2e^-$ ORR volcano plot. Moreover, the introduction of Mo species simultaneously suppresses the electroreduction of as-obtained $H_2O_2$ on Co sites. Owing to the integration of mesoporous hollow merits and electron-donating effect, the Co/Mo-MCHS electrocatalyst displays efficient $2e^-$ ORR pathway with a noticeable ring current response and high $H_2O_2$ selectivity of 90–95% over the wide potential range in acid. After long-term operation over 15 h, 90% of the initial $H_2O_2$ selectivity could be retained. For large-scale electrolysis, a remarkable $H_2O_2$ yield of 2102 mg for 150 h is obtained, suggesting great potential for practical applications. This study provides valuable guidance for the rational design of more complex SACs/carbon catalysts by combing different effects in the future.

*3.4.3 Coupling electronic defects with atomic active sites*

Liu *et al.*[154] systematically investigated a series of metals catalysts anchored on nitrogen-doped carbon (M−NC), including representative transition metals (Mn, Fe, Co, and Ni), 4*d* transition metal (Ru), 5*d* transition metal (Pt), and non-transition metal (In), to assess their activity for synthesizing $H_2O_2$ (**Figure 15**). Four types of M−NC catalysts with different pyridine and pyrrole N atoms ratios were constructed (**Figure 15**a). The $2e^-$ ORR activity volcano plot for total 40 SAC configurations were examined through DFT calculations (**Figure 15**b). The coordination environment can tune the $\Delta G_{*OOH}$ position in M−NCs significantly, with the highest value occurred at $MN_{(Po)4}$ type catalysts for each metal. Meanwhile, the corresponding $\Delta G_{*OH}$ and $2e^-$ WOR volcano curve were also calculated (**Figure 15**c), demonstrating that pyrrolic-N affect the adsorption of OH, and the free energy shift is almost consistent with *OOH. Considering the ORR and WOR reaction pathway together, the $CoN_{(Po)4}$, $MnN_{(Pd)1}N_{(Po)3}$ and $RuN_{(Po)4}$ show promising prospects as bifunctional SAC for $H_2O_2$ generation.

Considering the fitting curve of $\Delta G_{*OH}$ and $\Delta G_{*OOH}$ (**Figure 15**d) and all key factors including overpotential, reaction kinetics, transition state energy, and thermodynamic stability, $RuN_{(Po)4}$ SAC are the most promising candidate for efficient $H_2O_2$ generation, and the pyrrole N coordination can modulate the $2e^-$ ORR/WOR kinetics (**Figure 15**e). This study provides deep theoretical insights into regulating coordination structure for the rational design of high-efficient and stable bifunctional SACs/carbon catalysts for $H_2O_2$ production.

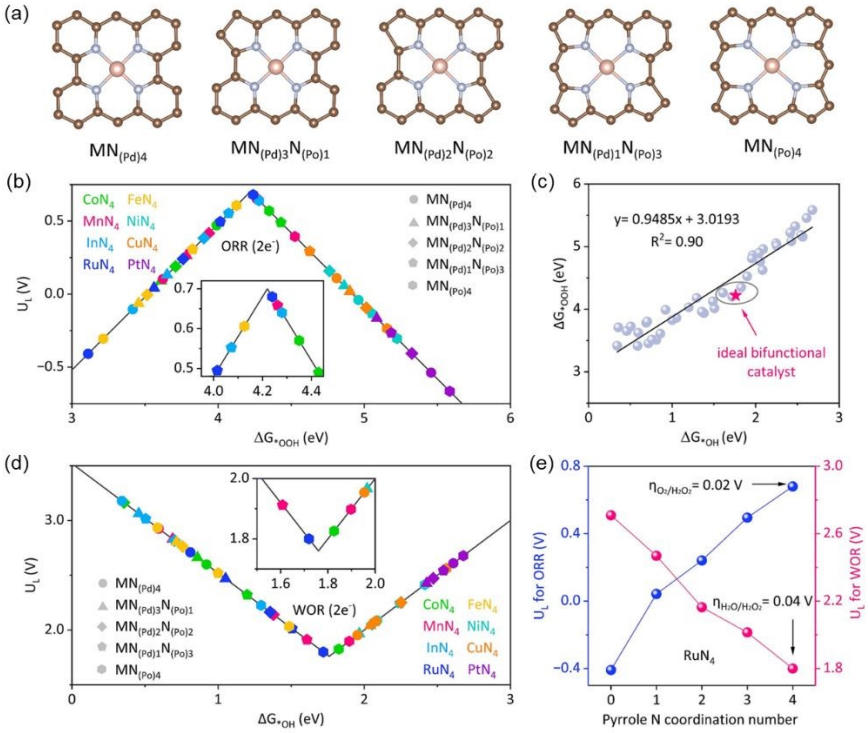


**Figure 15.** DFT calculation on various metal SAC catalysts anchored on nitrogen-doped carbon (M-NC) for $H_2O_2$ production via $2e^-$ ORR and $2e^-$ WOR. (a) Optimized $MN_4$ structure with different pyrrole N coordination numbers; Activity volcano relation for (b) $2e^-$ ORR and (c) $2e^-$ WOR between intermediates formation energy and limiting potential; (d) Scaling plots between $\Delta G_{*OH}$ and $\Delta G_{*OOH}$; (e) Relationship between pyrrole N coordination numbers and limiting potential for $2e^-$ ORR and $2e^-$ WOR of all Ru-NC catalysts. Reproduced with permission.[154] Copyright 2023, Elsevier.

### *3.4.4 Multiple synergistic effects*

The integration of multiple effects creates a powerful synergistic platform that overcomes the limitations of binary coupling, which can further maximize the overall catalytic efficiency. A representative example involves the rational design of highly porous open carbon nanocages

View Article Online
DOI: 10.1039/D5MH00221D

673 with embedded Co nanoparticles (NPs) fabricated through a template-assisted method. The
674 optimized P-Co@C-700 catalyst exhibits several intergrating effets, including highest
675 percentage of –C–O–C group and defects, embedding Co NPs, and mesoporous structure,
676 resulting in a high selectivity up to 94% toward $H_2O_2$ production in 0.1 m $HClO_4$. Benefiting
677 from the synergistically modulated electronic and pore structure, the optimized open carbon
678 nanocages exhibit outstanding activity, selectivity, and stability for $2e^-$ $H_2O_2$ production in
679 acidic condition.

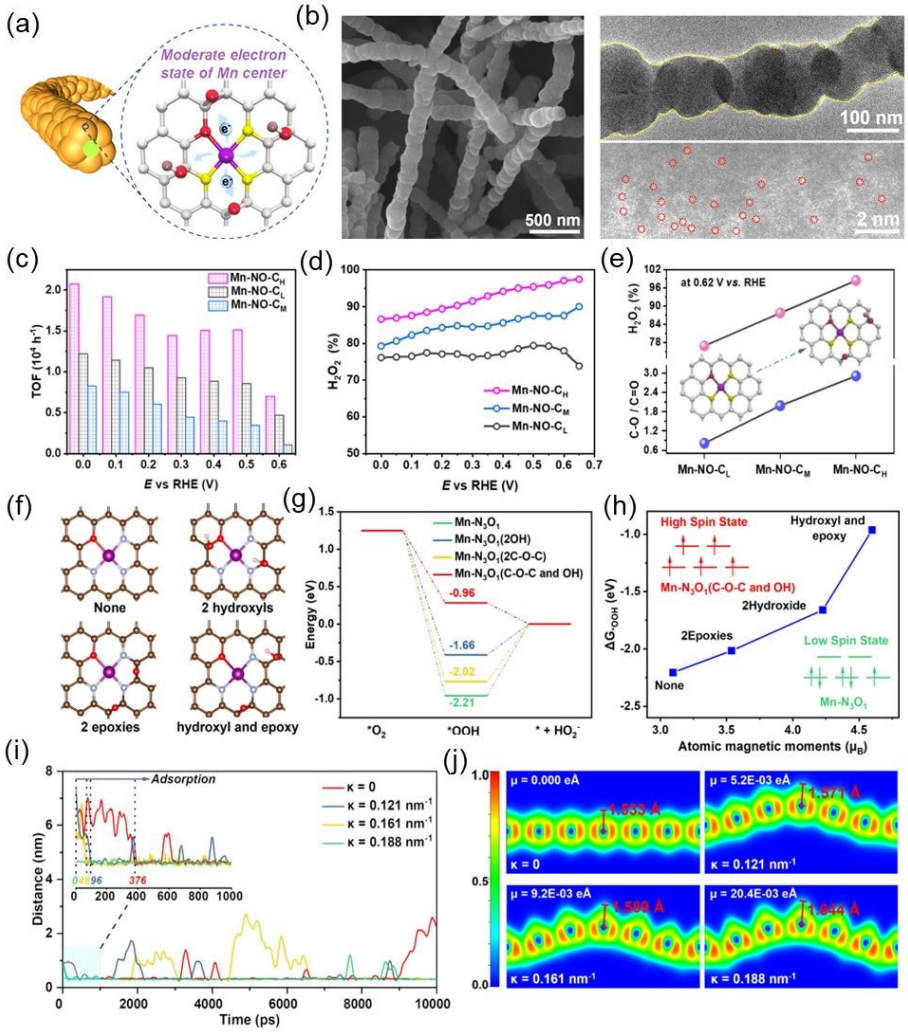


680

681 **Figure 16.** (a) The schematic of heterogeneous catalyst composed of boundary-rich carbons
682 supported active Mn(II) centers (Mn−NO−$C_H$) with selective oxygen functional groups. (b)
683 SEM, TEM and HAADF-STEM images of Mn−NO−$C_H$. (c) TOFs, (d) $H_2O_2$ selectivity, and
684 (e) correlation between $H_2O_2$ selectivity (0.62 V vs. RHE) and the proportion of oxygen species.
685 (f) The DFT models for Mn−$N_3O_1$. (g) The calculated free energy at 0 V vs. RHE for 2e-ORR
686 pathway. (h) The correlation between magnetic moment and the free energy for Mn−$N_3O_1$ after
687 *OOH adsorption. (i) MD simulation for the minimum distance between $O_2$ molecules and C

View Article Online
DOI: 10.1039/D5MH00221D

atoms. (j) Electronic Localization Function mapping images with different curvatures. Reproduced with permission.[143] Copyright 2024, Wiley-VCH.

Moreover, as a notable example, Dong *et al*.[143] developed a novel Mn SACs-coordinated boundary-rich porous carbon-based electrocatalysts (**Figure 16**a and b), in which the secondary coordinated epoxide, hydroxyl groups surrounding the Mn−$N_3$−O centers, and the boundary-rich morphology together lead to the predominant selectivity and efficiency for $H_2O_2$ production through the 2e⁻ ORR pathway. The catalysts exhibited nearly 100 % Faradaic efficiency and with a reaction rate up to 15100 mmol $g_{cat}^{-1}$ $h^{-1}$ (0.1 V *vs*. RHE), achieving the record activity for Mn-based electrocatalyst for electrosynthesis of $H_2O_2$ (**Figure 16**c-e). Mechanistic investigations indicate that the epoxide and hydroxyl groups surrounding the Mn(II) centers promote spin state and tailor the adsorption of *OOH intermediate, and multiscale simulations reveal that the high-curvature boundaries can promote adsorption and local enrichment of $O_2$ (**Figure 16**f-j). Such synergy highlights the importance of holistic material design, where defects, doping, and atomic-scale engineering work in concert to achieve greatly improved performance.

To comprehensively evaluate the advantages and limitations of carbon-based electrocatalysts for $H_2O_2$ production, it is essential to compare them with non-carbon-based catalyst systems, such as metal oxides and noble-metal catalysts. **Table 1** summarizes the critical metrics (onset potential, $H_2O_2$ selectivity, production rate, and stability) across different representative catalyst types. Although Pt/Pd-based noble metal-based catalysts are recognized as efficient catalysts with small overpotential and high selectivity for 2e⁻ ORR, their industrial-scale application is greatly limited by scarcity, high cost, and susceptibility to poisoning.[24, 41, 156, 157] Metal oxide electrocatalysts demonstrate excellent stability, while achieving high selectivity remain challenging.[158] Although some recently reported metal oxides such as *h*-$SnO_2$ demonstrate superb electrocatalytic activity,[159] but still surfer from poor stability in electrolyte. Furthermore, synthesizing high active metal oxide catalysts often requires complex procedures and precise

View Article Online
DOI: 10.1039/D5MH00221D

control over their structure and composition. It is also worth noting that the emerging MOF/COF materials show high production activity but poor stability.

We have summarized the most representative carbon-based materials for electrocatalytic $H_2O_2$ production reported in the past few years (**Table 2**), systematically classified by materials design categories: microstructure tailoring, defect engineering (including intrinsic and heteroatom doping), surface functional group modulation, and single-atomic site configurations. In comparison, carbon-based electrocatalysts offer distinct advantages, including low-cost and widely availability, making them highly attractive for large-scale applications. Up till now, the performance of carbon-based electrocatalyst is comparable or even outperforming many noble metal-based systems, maintaining cost and environmental benefits. Carbon-supported single-atom catalysts (SACs) achieve high production rates of ~500–30,000 $mmol \cdot g^{-1} \cdot h^{-1}$. However, the activity and stability of carbon catalysts in neutral or weakly acidic environments still needs to be further improved, as well as mitigating degradation during long-term electrochemical operation.

The stability of carbon-based electrocatalysts for $H_2O_2$ production varies significantly across different categories, with durations ranging from a few hours to ~250 h. Microstructure-modulated catalysts like graphitic ordered mesoporous carbon (O-GOMC) exhibit high stability (168 h) due to robust porous frameworks, while defect-engineered materials such as B-doped carbon demonstrate durability (100 h) under high current densities. Surface modifications, including polymer coatings or metal complexes, demonstrated relatively low stability as evidenced by CoPc-carbon (24 h). Although single-atom catalysts generally exhibit very short liftime (~10 h), recently reported synergistic systems such as Pb SAs/OSC (100 h) and N,S-rich carbon nanotubes (200 h) are highly promising. Challenges still remain in standardizing testing protocols and achieving long-term stability for industrial applications. Future research should focus on elucidating degradation mechanisms and optimizing catalyst designs for extended operational lifetimes.

View Article Online
DOI: 10.1039/D5MH00221D

**Table 1.** Comparison of performance with representative non-carbon-based systems.

| Type | Catalysts | Selectivity (%) | $H_2O_2$ production rate | Electrolyte | Stability | Ref. |
|---|---|---|---|---|---|---|
| Noble metals | $PtP_2$ | 98.5 | 2.26 mmol·$h^{-1}$·$cm^{-2}$ | 0.1 M $HClO_4$ | 120 h | 160 |
| | Pt-Hg/C | >90 | / | 0.1 M $HClO_4$ | 8000 cycles | 24 |
| | $Pt_1$-$CuS_x$ | 92–96 | 546 mmol·$g^{-1}$·$h^{-1}$ | 0.1 M $HClO_4$ | 10 h | 161 |
| | $Pt_1/CoSe_2$ | / | 110.02 mmol·$g^{-1}$·$h^{-1}$ | 0.1 M $HClO_4$ | 60 h | 162 |
| Oxides | h-$SnO_2$ | 99.9 | 3885.26 mmol·$g^{-1}$·$h^{-1}$ | 0.1 M $Na_2SO_4$ | 20 h | 159 |
| | α-$Fe_2O_3$ | 80.5 | 546.8 mmol·$g^{-1}$·$h^{-1}$ | 0.1 M KOH | 48 h | 158 |
| Carbon-based | Single atoms-carbon | 96.5 | 12510 mmol·$g^{-1}$·$h^{-1}$ | 0.1 M KOH | 12 h | 163 |
| | N/S-CNTs | 90.0 | 30370 mmol·$g^{-1}$·$h^{-1}$ | 1.0 M KOH | 200 h | 164 |
| | B-doped carbon | 88.7 | 24300 mmol·$g^{-1}$·$h^{-1}$ | 0.1 M KOH | 100 h | 165 |
| Other systems | MOF nanosheets | 99 | 6500 mmol | 0.1 M KOH | 11 h | 166 |
| | Boron nanosheets | ~90 | 25100 mmol $g^{-1}$ $h^{-1}$ | 1.0 M $Na_2SO_4$ | 140 h | 167 |

744 **Table 2.** Summary of representative carbon-based materials for electrocatalytic $H_2O_2$ production.

| Type | Catalysts | Electrolyte | Onset potential (V vs. RHE) | $H_2O_2$ selectivity (%) | Production rate | Voltage (V vs. RHE) | Faradaic efficiency (%) | Tafel slope ($mV \cdot dec^{-1}$) | Stability | Ref. |
|---|---|---|---|---|---|---|---|---|---|---|
| Microstructure modulation | Carbon mesoporous nanoreactors (MHCS) | 0.1 M KOH | 0.6 | 85 | 3.36 $mmol \cdot L^{-1} \cdot h^{-1}$ | 0.5 | 97 | 73 | 12 h | 168 |
| | Graphitic ordered mesoporous carbon (O-GOMC) | 0.1 M KOH | 0.75 | ~92 | 63.33 $mg \cdot L^{-1} \cdot h^{-1}$ | 0.6 | 99.2 | 42 | 168 h | 169 |
| | O-GOMC | 0.1 M KOH | 0.73 | 93±1 | 24 $mmol \cdot L^{-1}$ | / | 99 | 59 | 16 h (3 mA) | 170 |
| | Honeycomb carbon nanofibers (HCNFs) | 0.1 M KOH | 0.87 | 97.3 | 6.37 $mmol \cdot L^{-1} \cdot h^{-1}$ (0.05 mg) | 0.5 | / | 75.6 | 12 h | 171 |
| | Porous carbon ($PCC_{900}$) | 0.1 M KOH | 0.83 | 95 | 1696.8 $mmol \cdot g^{-1} \cdot h^{-1}$ | / | 90 | 38 | 10000 times | 172 |
| | Hollow mesoporous carbon sphere (HMCSs) | 0.1 M KOH | 0.82 | 95 | / | 0.53 | 87 | / | 10 h | 173 |
| | Mesoporous carbon-nanofibers (MCNF) | 0.1 M KOH | 0.68 | >90 | / | 0.4 | >85 | 43 | 12 h | 174 |
| | Holey graphene | 0.1 M KOH | 0.56 | 95 | 2360 $mmol \cdot g^{-1} \cdot h^{-1}$ | 0.1 | 97 | / | 12 h | 175 |
| | Oxidized carbon nanotubes | 0.1 M KOH | 0.795 | >90 | / | 4 | >85 | 38 | 96 h | 176 |
| | Oxygen-doped carbon quantum dots | 0.1 M KOH | / | 96.2 | 338.7 $mmol \cdot g^{-1} \cdot h^{-1}$ | -1.33 | 92 | 66.95 | 120 h | 177 |
| Defect engineering | Oxygen modified defective graphene | 0.1 M KOH | 0.9 | 98.38 | 41.45 $mg \cdot cm^{-2} \cdot h^{-1}$ | 0.5 | 95 | / | 10 | 178 |
| | Doped carbon nanohorns | 0.1 M KOH | 0.85 | >80 | 740 $mmol \cdot g^{-1} \cdot h^{-1}$ | 0.65 | 50-100 | 49 | 12 h | 179 |
| | B-doped carbon | 0.1 M KOH | 0.780 | 88.7 | 24300 $mmol \cdot g^{-1} \cdot h^{-1}$ | / | 82 | 51 | 100 h (100 $mA \cdot cm^{-2}$) | 165 |
| | B-doped nanocarbon | 0.1 M KOH | 0.78 | 95 | 247 $mg \cdot L^{-1} \cdot h^{-1}$ | 0.5 | 100 | / | 10 h | 180 |

| | | | | | | | | | | |
|---|---|---|---|---|---|---|---|---|---|---|
| | B-doped carbon | 0.1M KOH | 0.773 | 95 | 7.36 $mmol \cdot cm^{-2} \cdot h^{-1}$ | / | 90 | 78 | 30 h (200 $mA \cdot cm^{-2}$) | 181 |
| | N-doped carbon spheres | 0.1 M KOH | 0.7 | 91.9 | 618.5 $mmol \cdot g^{-1} \cdot h^{-1}$ | 0.4 | 85.1 | / | 10 h | 182 |
| | N-doped graphene | 0.1 M KOH | 0.764 | >82 | 224.8 $mmol \cdot g^{-1} \cdot h^{-1}$ | 0.3 | >43.6 | / | 4 h | 183 |
| | N-doped carbon | 0.1 M $HClO_4$ | 0.6 | 80-98 | 2923 $mg \cdot L^{-1} \cdot h^{-1}$ | 0.3 | 100 | 136.6 | 10 h | 184 |
| | N-doped carbon | 0.5 M NaCl | 0.61 | 95 | 631.2 $mmol \cdot g^{-1} \cdot h^{-1}$ | 0.51 | 79.8 | 79 | 10 h | 185 |
| | N,O co-doped carbon nanosheets | 0.1 M $K_2SO_4$ | 0.65 | >90 | 6705 $mmol \cdot g^{-1} \cdot h^{-1}$ | 0.2 | 91 | 52 | 24 h | 186 |
| | Polydopamine modified carbon (CB-PDA-A) | 0.1 M KOH | 0.8 | 80 | 1800 $mmol \cdot g^{-1} \cdot h^{-1}$ | 1.5 | 95 | 70 | 250 h | 61 |
| | CoPc-carbon | 0.1 M KOH | 0.7 V | 99% | 10400 $mmol \cdot g^{-1} \cdot h^{-1}$ | 0.2 | 93 | 54 | 24 h | 187 |
| Surface modification | Polymerization of acrylonitrile (PNAC-F) | 0.1 M KOH | 0.78 | 93 | 816 $mmol \cdot g^{-1} \cdot h^{-1}$ | 0.78 | / | / | 40 h | 188 |
| | Carbon black | 0.1 M KOH | 0.75 | 96 | / | 0.33 | / | 60 | 10 h | 189 |
| | Activated coke@carbon cloth | 0.1 M $Na_2SO_4$ | / | 100 | 30.41 $mg \cdot h^{-1} \cdot cm^{-2}$ | / | 80 | 104.1 | 10 h | 190 |
| | N-B-OH-Graphene quantum dots | 0.1 M KOH | 0.7 | 90 | 709 $mmol \cdot g^{-1} \cdot h^{-1}$ | 0.2 | 81 | / | 12 h | 191 |
| | Pb-carbon dot (Pb SAs/OSC) | 0.10 M KOH | 0.65 | >90 | 6.9 $mmol \cdot cm^{-1} \cdot h^{-1}$ | / | 92.7 | 49 | 100 h (50 $mA \cdot cm^{-2}$) | 192 |
| | Single atoms cellulose-carbon (FeSAs/ACs-BCC) | 0.1 M KOH | 0.78 | 96.5 | 12510 $mmol \cdot g^{-1} \cdot h^{-1}$ | 0.4 | 89.4 | 73 | 12 h | 163 |
| Single-atom/cabron hybrids | In single atoms on carbon (In SAs/NSBC) | 0.1 M KOH | 0.66 | 95 | 6490 $mmol \cdot g^{-1} \cdot h^{-1}$ | 0.3 | 75 | 30.3 | 12 h | 193 |
| | Pt single atoms-g-$C_3N_4$ ($Pt_{0.21}$/CN) | 0.1 M KOH | 0.81 | 98 | 767 $mmol \cdot g^{-1} \cdot h^{-1}$ | 0.6 | 96 | / | 10 h | 194 |

| | | | | | | | | | | |
|---|---|---|---|---|---|---|---|---|---|---|
| | Metal-nitrogen-carbon | 0.1 M $HClO_4$ | 0.75 | >70 | 688 $mmol \cdot g^{-1} \cdot h^{-1}$ | 0.3 | 93 | 113 | 12 h | [195] |
| | CoZn-N/O-carbon nanotube ($CoZn_{SA}$@CNTs) | 0.1 M KOH | / | 90-100 | 4770 $mmol \cdot g^{-1} \cdot h^{-1}$ | 0.2 | 95 | 76.3 | 5 h | [196] |
| | Co-$O_4$ porous graphene-like carbon (Co-$O_4$@PC) | 0.1 M KOH | 0.73 | 98.8 | 250 $mmol \cdot g^{-1} \cdot h^{-1}$ | 0.5 | / | 72 | 10 h | [197] |
| | Co-$N_4$, C-O-C epoxide groups | 0.1 M KOH | 0.801 | 91.3 | 6912 $mmol \cdot g^{-1} \cdot h^{-1}$ | 0.09 | / | 51.3 | 10 h | [198] |
| | Atomic metal-nitrogen-carbon (F/Co-N-G SAC) | 0.1 M KOH | 0.810 | 94.2 | 12100 $mmol \cdot g^{-1} \cdot h^{-1}$ | 0.1 | 70 | 45.2 | 10 h | [199] |
| | S,N-coordinated Ni SAC (Ni-$N_3S$) | 0.1 M KOH | 0.80 | 90.0 | 17500 $mmol \cdot g^{-1} \cdot h^{-1}$ | 0.2 | 85 | / | 12 h | [200] |
| | Bipyridyl N-carbonyl (Pd-$N_2O_2$-C) | 0.1 M KOH | 0.82 | 95 | 1.5×107 $mmol \cdot g^{-1} \cdot h^{-1}$ | 0.4 | / | / | 10 h | [201] |
| Synergistic effects | Pd atoms on nitrogen-doped carbon (Pd-NC) | 0.1 M KOH | 0.8 | 95 | 30 $mmol \cdot g^{-1} \cdot h^{-1}$ | 0.5 | / | 56 | 8 h | [202] |
| | Carbon-based single atom (Zn-$N_2O_2$-S SAC) | 0.1 M KOH | / | 96 | 6924 $mmol \cdot g^{-1} \cdot h^{-1}$ | / | 93.1 | 62 | 65 h (80 $mA \cdot cm^{-2}$) | [203] |
| | Co SACs-carbon nanofiber (Co@EO-ACNF) | 0.1 M KOH | / | 85.21 | 15750 $mmol \cdot g^{-1} \cdot h^{-1}$ | 0.6 | 84.5 | / | 48 h | [204] |
| | W SAC on O,N-doped carbon ($W_1$/NO-C) | 0.1 M KOH | 0.815 | >90 | 1230 $mmol \cdot g^{-1} \cdot h^{-1}$ | 0.6 | 95 | 115 | 20 h | [205] |
| | Pd-oxidized carbon nanotubes | 0.1 M $HClO_4$ | 0.7 | 95 | 1700 $mmol \cdot g^{-1} \cdot h^{-1}$ | 0.1 | 93 | / | 8 h | [74] |
| | Defective carbon (Mo-CDC-ns) | 0.1 M KOH | 0.75 | 90 | 455 $mmol \cdot g^{-1} \cdot h^{-1}$ | 0.55 | 85.1 | 95-99 | 12 h | [206] |
| | Co@carbon nanocages | 0.1 M $HClO_4$ | 0.60 | 94 | 57 $mmol \cdot g^{-1} \cdot h^{-1}$ | 0.31 | / | 107.9 | 10 h | [207] |

| | | | | | | | | | | |
|---|---|---|---|---|---|---|---|---|---|---|
| | Ni SAC-carboxyl-multiwall carbon nanotubes ($N_4Ni_1O_2$/OCNTs) | 1 M KOH | 0.68 | / | 5.7 $mmol \cdot cm^{-2} \cdot h^{-1}$ | / | 96.1 | 107 | 24 h (200 $mA \cdot cm^{-2}$) | 208 |
| | Oxygen-vacancy-graphene armor (B/N-HCNS@V-G) | 1 M KOH | 0.79 | 91 | 55 ppm | 0.5 | 94 | 63 | 24 h | 209 |
| | Carbon nanotubes with N,S-rich tips (N, S-TCNTs) | 1 M KOH | 0.78 | 90.0 | 30370 $mmol \cdot g^{-1} \cdot h^{-1}$ | / | >90 | 55.5 | 200 h (100 mA) | 164 |

745

View Article Online
DOI: 10.1039/D5MH00221D

## 4. Conclusions and perspective

The electrochemical production of $H_2O_2$ using carbon-based nanomaterials has gained considerable research attention as an environmentally friendly, low-cost and efficient method. Substantial efforts have been made both experimentally and theoretically on $2e^-$ ORR electrocatalysis, with a focus on the structural-property relation and design of efficient carbon-based electrocatalysts. In this review, we summarized the key advancements in the materials design strategy. These studies demonstrate that modifying the local atomic structure of carbon materials, incorporating functional surface groups, doping with foreign atoms, tailoring microstructure, and introducing semiconductor or single-atomic sites can enhance not only the activity and selectivity for $H_2O_2$ production but also the long-term stability of these catalysts. These developments open the door to more efficient and scalable electrocatalytic processes for green $H_2O_2$ production.

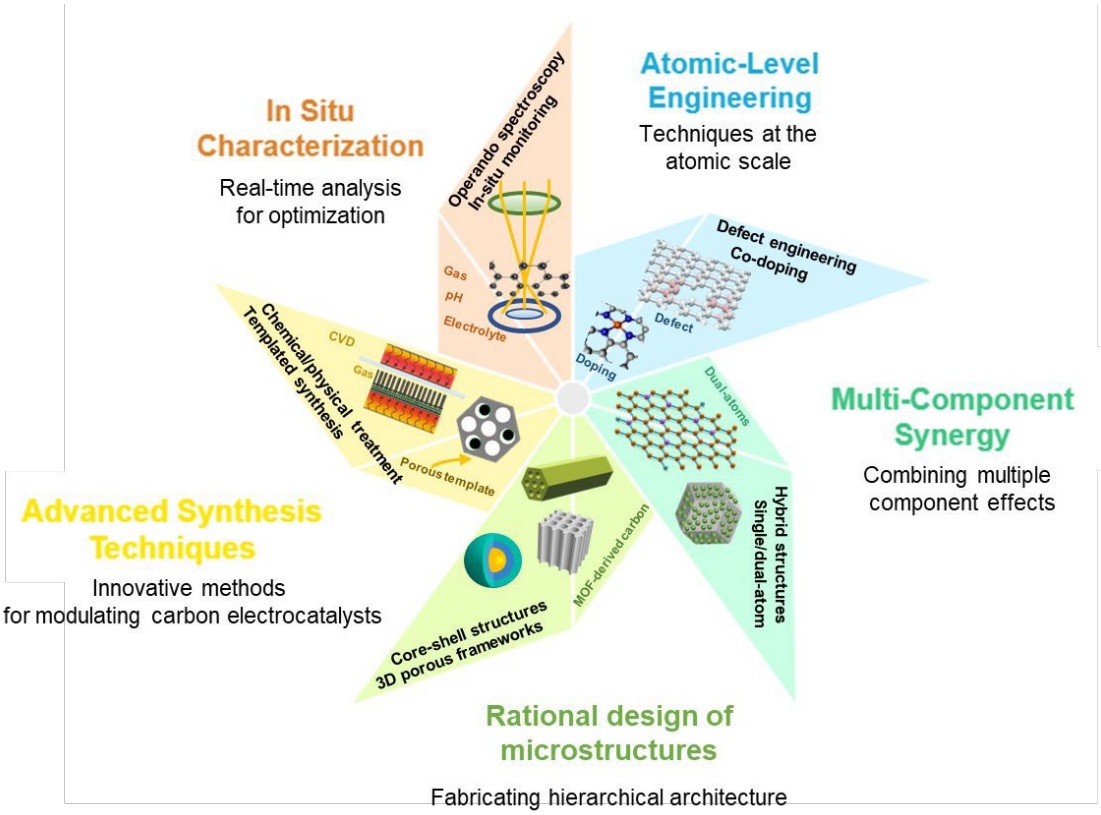


**Figure 17.** Schematic of perspective strategizes for rational design of carbon catalysts (atomic level engineering, multiple-synergistic effects), advanced synthesis method, and in-situ characterization techniques.

View Article Online
DOI: 10.1039/D5MH00221D



Despite the considerable progress achieved, challenges remain for the industrial-scale implementation of electrocatalytic $H_2O_2$ production using carbon-based materials, including improving electrocatalytic activity, ensuring long-term stability, and developing practical designs for carbon-based electrodes and reactors. Therefore, advancing carbon electrocatalyst design to achieve high activity and selectivity has become a primary focus in this field. Furthermore, innovation in catalyst preparation, optimization of the activity and selectivity, as well as deeper understanding of mechanisms are crucial to further advancing $H_2O_2$ production in an environmentally benign manner more effectively. To date, carbon-based electrocatalysts has demonstrated remarkable progress, driven by advances in engineering strategies that have significantly improved catalyst performance over traditional methods. In the following section, we will summarize and discuss the challenges and future perspectives in this research area (**Figure 17**), including the rational design of carbon catalysts (e.g., atomic level engineering, multiple-synergistic effects), advanced synthesis method, in-situ characterization techniques, and system-level device design considerations for industrial applications.

The catalytic activity of carbon-based materials still has significant potential for further improvement. Multiple synergistic modification strategies can be employed, including defect engineering (e.g., creating vacancies and edge sites to promote $O_2$ adsorption), chemical doping (e.g., introducing N, B, or S heteroatoms to tune electronic structure), facet control (e.g., exposing specific crystal planes with optimal *OOH intermediate binding energy), surface active site design (e.g., atomically dispersed metal-$N_4$ moieties), interface engineering (e.g., constructing hybrid metal oxide/carbon junctions to facilitate charge transfer), and microstructural modulation (e.g., developing hierarchically porous architectures to improve mass transport). Although existing strategies have made notable progress in the electrosynthesis of $H_2O_2$, the precise control of defects and single-atomic sties in carbon materials requires further investigation to optimize the balance between the intrinsic activity and selectivity of

View Article Online
DOI: 10.1039/D5MH00221D

active sites. To precisely engineer defects in carbon-based materials, several methodologies can be utilized: (1) plasma irradiation (Ar, $N_2$, or $O_2$) for controlled introduction of vacancies and edge defects; (2) mechanical exfoliation techniques such as ball-milling or ultrasonication to create strain-induced defects; and (3) pyrolysis of metal-organic frameworks (MOFs) to derive defect-rich carbon matrices with atomic-level precision. Moreover, to promote mass transfer process, tailoring the morphology of the catalysts with well-designed 3D hierarchically porous architectures can significantly increase the availability of active sites and accelerate the diffusion of reactants. The pore sizes and distribution need to be carefully designed to balance the retention time and selective $H_2O_2$ production, reactant diffusion, resistance and reaction kinetics. Specific methods include the use of sacrificial templates (e.g., mesoporous silica, PMMA spheres, and amphiphilic block copolymers), combine with resins (e.g., resorcinol-formaldehyde) for ordered mesopores, or add macroporogen (e.g., emulsion droplets) for triple porosity. In addition, it is crucial to introuduce surface functional groups (e.g., -COOH or -OH) to tune hydrophilicity for improving electrolyte accessibility and modifying intermediate binding strength through dipole interactions. For single-atom carbon catalysts, the uncontrollable selectivity and poor stability remain critical challenges. The implement of atomic layer deposition (ALD) for depositing protective layer (e.g., $Al_2O_3$ or $TiO_2$ sub-nanolayers) can be used to enchance the stabliity while allowing reactant access; creating proximal dual-atom sites is effective to promote the selectivity by modulating the O-O bond cleavage. Critically, the synergistic integration of these strategies represents a pivotal research direction for achieving sustained high selectivity in the $2e^-$ oxygen reduction pathway. Beyond catalyst design, the role of the electrolyte in $H_2O_2$ production also deserves attention, as it can influence the stability of the key intermediate *OOH, thereby regulating the overall efficiency of $H_2O_2$ formation. And the ORR activity through the $2e^-$ pathway remains limited for many carbon-based materials in neutral or weakly acidic environments.

Beyond materials design, elucidating the fundamental electrocatalytic mechanisms remains a critical research priority. At this moment, the reaction mechanisms of carbon-based electrocatalysts remain insufficiently understood. It is worth noting that the active sites in carbon catalysts typically undergo dynamic evolution during electrochemical reactions, necessitating the study of these changes to fully explore the reaction mechanisms. To this end, a comprehensive understanding of reaction pathways, active site dynamics under operational conditions, and interfacial phenomena is essential for rationally guiding catalyst optimization. Therefore, various in-situ/operando characterization techniques are needed to directly probe reactive intermediates, active sites, and their interactions during electrochemical $H_2O_2$ generation process. For instance, in-situ XRD and X-ray absorption spectroscopy (XAS) can be employed to analyze the local coordination environment, electronic structure, and oxidation state of catalysts in real time. In addition, in-situ Raman and FTIR spectroscopy are valuable for real-time detection of reaction intermediates during electrocatalysis reactions. Further improvement in spatial and temporal resolution for in situ detection of dynamic electrocatalytic processes is also desirable. To gain deeper insights into electrocatalytic mechanisms, advanced theoretical calculations are needed to quantitatively correlate the energetics of intermediates with reaction kinetics. With ongoing advances in computational power, algorithms, and big data from both experiments and simulations, machine learning could play a transformative role in predicting structure-performance relationships at previously unattainable scales. At present, the $2e^-$ WOR has received less attention and is in its early stages of development compared to the $2e^-$ ORR. Thus, the development of novel computational approaches to screen and guide the design of advanced carbon-based $2e^-$ WOR electrocatalysts is essential. A fundamental mechanistic understanding will elucidate the critical interplay between: (1) reaction intermediate energetics, (2) surface-dependent selectivity determinants (e.g., *OOH binding strength, local coordination environments), and (3) electrochemical microenvironment effects

View Article Online
DOI: 10.1039/D5MH00221D

(pH, potential, double-layer structure), ultimately enabling rational design of efficient $H_2O_2$ production systems.

While catalyst design has advanced significantly, it is worth noting that the development of electrochemical reactors has lagged behind catalyst design in the past decade. Therefore, system-level optimization is essential for practical implementation of carbon-based electrocatalysts. Particular emphasis should be placed on the design of the overall electrochemical system and the operational reliability of the industrial-grade device for practical applications. Key considerations include $O_2$ mass transfer, device design, electrolyte selection, ion exchange membranes, and reactor configurations. First, the mass transfer and diffusion of reactant species within the interface microenvironment of the carbon electrode needs further investigation.[210] Specific optimization strategies involve gas diffusion electrodes with hierarchical porosity (macro/meso/micro pores) to balance $O_2$ transport and flow-through membrane reactors with rotational cathodes. The use of porous solid electrolyte (PSE) reactor for producing high-concentration and high-purity $H_2O_2$ may meet the high stability requirment.[211] In addition, optimizing local reaction environments—such as water permeation/wetting, hydrophobicity/hydrophilicity, and reactant concentration—can enhance the performance of carbon-based electrocatalysts. Significant research efforts should focus on advancing reactor engineering, particularly for flow cell configurations and dual-PEM solid electrolyte systems. These reactor designs must simultaneously address two critical challenges: (1) corrosion resistance against both acidic/alkaline electrolytes and concentrated $H_2O_2$ (up to 10 wt%), and (2) maintenance of stable three-phase interfaces under industrial current densities (>200 $mA \cdot cm^{-2}$). Innovative architectures incorporating corrosion-resistant materials (e.g., PTFE-coated titanium flow fields, stabilized carbon-PTFE gas diffusion electrodes) and optimized hydrodynamics are crucial for achieving economically viable $H_2O_2$ electrosynthesis at large scale. Furthermore, the $H_2O_2$ products are typically generated in a mixture, with solutes in traditional liquid electrolytes ranging from acidic to alkaline pH. Extra separation processes

to recover pure $H_2O_2$ solutions are therefore required. Using a solid-state electrolyte can avoid contamination of the product solution by extraneous ions.[2] Producing $H_2O_2$ in neutral solutions offers practical advantages by avoiding pH-related complications, such as electrode degradation or the need for neutralization steps. Seawater, as an abundant and naturally neutral electrolyte, directly supports this goal by providing a sustainable medium for electrochemical $H_2O_2$ production via the $2e^-$ ORR pathway. The dissolved oxygen serves as a reactant for carbon-based electrocatalysts, which have demonstrated high efficacy in neutral media. Moreover, the use of seawater eliminates the costs and environmental impacts associated with synthetic pH adjustments, enhancing both scalability and the sustainability of the process. However, challenges such as chloride interference may compromise catalyst stability and selectivity, necessitating the development of robust carbon-based materials and more in-depth mechanistic studies in simulated seawater electrolytes to fully realize these benefits. Consequently, exploring suitable and stable carbon-based catalysts and understanding the catalytic mechanism in neutral simulated seawater electrolytes is an urgent and promising area of research.[212] Moreover, sustainable $H_2O_2$ production coupled to the high value added chemical synthesis are worth exploring, such as oxidative valorization of glycerol[213] and cellulosic biomass upgrading into valued formic acid.[214]

**Acknowledgements**

This work was supported by financial aid from the National Natural Science Foundation of China (Grant No. 22075126 and 52172187), the Start-up funding for Jinshan Distinguished Professor of Jiangsu University, and the Jiangsu Provincial Senior Talent Program (Dengfeng).

**Conflicts of interest**

There are no conflicts to declare.

View Article Online
DOI: 10.1039/D5MH00221D





## References:


1. R. Ciriminna, L. Albanese, F. Meneguzzo and M. Pagliaro, *ChemSusChem*, 2016, **9**, 3374-3381.
2. S. C. Perry, D. Pangotra, L. Vieira, L.-I. Csepei, V. Sieber, L. Wang, C. Ponce de León and F. C. Walsh, *Nat. Rev. Chem.*, 2019, **3**, 442-458.
3. J. A. Dowling, K. Z. Rinaldi, T. H. Ruggles, S. J. Davis, M. Yuan, F. Tong, N. S. Lewis and K. Caldeira, *Joule*, 2020, **4**, 1907-1928.
4. O. C. Esan, X. Shi, Z. Pan, Y. Liu, X. Huo, L. An and T. S. Zhao, *J. Power Sources*, 2022, **548**, 232114.
5. J. M. Campos-Martin, G. Blanco-Brieva and J. L. G. Fierro, *Angew. Chem. Int. Ed.*, 2006, **45**, 6962-6984.
6. A. G. Fink, R. S. Delima, A. R. Rousseau, C. Hunt, N. E. LeSage, A. Huang, M. Stolar and C. P. Berlinguette, *Nat. Commun.*, 2024, **15**, 766.
7. S. J. Freakley, Q. He, J. H. Harrhy, L. Lu, D. A. Crole, D. J. Morgan, E. N. Ntainjua, J. K. Edwards, A. F. Carley, A. Y. Borisevich, C. J. Kiely and G. J. Hutchings, *Science*, 2016, **351**, 965-968.
8. T. Ricciardulli, S. Gorthy, J. S. Adams, C. Thompson, A. M. Karim, M. Neurock and D. W. Flaherty, *J. Am. Chem. Soc.*, 2021, **143**, 5445-5464.
9. Y. Zhang, C. Pan, G. Bian, J. Xu, Y. Dong, Y. Zhang, Y. Lou, W. Liu and Y. Zhu, *Nat. Energy*, 2023, **8**, 361-371.
10. R. Liu, Y. Chen, H. Yu, M. Položij, Y. Guo, T. C. Sum, T. Heine and D. Jiang, *Nat. Catal.*, 2024, **7**, 195-206.
11. Z. Teng, Q. Zhang, H. Yang, K. Kato, W. Yang, Y.-R. Lu, S. Liu, C. Wang, A. Yamakata, C. Su, B. Liu and T. Ohno, *Nat. Catal.*, 2021, **4**, 374-384.
12. H. Tan, P. Zhou, M. Liu, Q. Zhang, F. Liu, H. Guo, Y. Zhou, Y. Chen, L. Zeng, L. Gu, Z. Zheng, M. Tong and S. Guo, *Nat. Synth*, 2023, **2**, 557-563.
13. Y. Shiraishi, T. Takii, T. Hagi, S. Mori, Y. Kofuji, Y. Kitagawa, S. Tanaka, S. Ichikawa and T. Hirai, *Nat. Mater.*, 2019, **18**, 985-993.
14. R. Pan, W. Lv, X. Ge, X. Huang, Q. Hu, K. Song, Q. Liu, H. Xie, B. Wu and J. Yuan, *Adv. Funct. Mater.*, 2025, **35**, 2414193.
15. Y. Liu, L. Li, Z. Sang, H. Tan, N. Ye, C. Sun, Z. Sun, M. Luo and S. Guo, *Nat. Synth.*, 2025, **4**, 134-141.
16. P. Sun, Z. Mo, J. Zhang, G. Wu, Z. Miao, K. Zhong, Y. Wei, C. Jia, Z. Chen and H. Xu, *Chem. Eng. J.*, 2023, **478**, 147337.
17. H. Jiang, L. Wang, X. Yu, L. Sun, J. Li, J. Yang and Q. Liu, *Chem. Eng. J.*, 2023, **466**, 143129.
18. C. Zhou, Y. Song, Z. Wang, J. Liu, P. Sun, Z. Mo, J. Yi and L. Zhai, *J. Environ. Chem. Eng.*, 2023, **11**, 110138.
19. W. Wang, L. Wang, L. Sun, H. Jiang, Y. Liu, Q. Liu, X. She and H. Tang, *Chem. Eng. J.*, 2023, **477**, 146945.
20. R. Chen, Z. Zhang, J. Wu, X. Chen, L. Wang, H. Yin, H. Li, J. Ding, H. Wan, G. Guan, *Renew. Energy*, 2022, **197**, 943-952.
21. Z. Lu, G. Chen, S. Siahrostami, Z. Chen, K. Liu, J. Xie, L. Liao, T. Wu, D. Lin, Y. Liu, T. F. Jaramillo, J. K. Nørskov and Y. Cui, *Nat. Catal.*, 2018, **1**, 156-162.
22. C. Xia, Y. Xia, P. Zhu, L. Fan and H. Wang, *Science*, 2019, **366**, 226-231.
23. E. Jung, H. Shin, B.-H. Lee, V. Efremov, S. Lee, H. S. Lee, J. Kim, W. Hooch Antink, S. Park, K.-S. Lee, S.-P. Cho, J. S. Yoo, Y.-E. Sung and T. Hyeon, *Nat. Mater.*, 2020, **19**, 436-442.
24. S. Siahrostami, A. Verdaguer-Casadevall, M. Karamad, D. Deiana, P. Malacrida, B. Wickman, M. Escudero-Escribano, E. A. Paoli, R. Frydendal, T. W. Hansen, I.

Chorkendorff, I. E. L. Stephens and J. Rossmeisl, *Nat. Mater.*, 2013, **12**, 1137-1143.
25. Y. Jiang, P. Ni, C. Chen, Y. Lu, P. Yang, B. Kong, A. Fisher and X. Wang, *Adv. Energy Mater.*, 2018, **8**, 1801909.
26. X. Sun, J. Yang, X. Zeng, L. Guo, C. Bie, Z. Wang, K. Sun, A. K. Sahu, M. Tebyetekerwa, T. E. Rufford and X. Zhang, *Angew. Chem. Int. Ed.*, 2024, **63**, e202414417.
27. D. Deng, J. Wang, M. Wang, Y. Wang, J. Jiang, Y. Chen, Y. Bai, Q. Wu and Y. Lei, *J. Mater. Sci. Technol.*, 2025, **227**, 76-81.
28. L. Cui, B. Chen, D. Chen, C. He, Y. Liu, H. Zhang, J. Qiu, L. Liu, W. Jing and Z. Zhang, *Nat. Commun.*, 2024, **15**, 10632.
29. J. Zhao, X. Zhang, J. Xu, W. Tang, Z. Lin Wang and F. Ru Fan, *Angew. Chem. Int. Ed.*, 2023, **62**, e202300604.
30. M. Ran, B. Du, W. Liu, Z. Liang, L. Liang, Y. Zhang, L. Zeng and M. Xing, *Proc. Natl. Acad. Sci.*, 2024, **121**, e2317435121.
31. S. Li, X. Zhang, F. Yang, J. Zhang, W. Shi and F. Rosei, *Chem Catal.*, 2024, **4**, 100901.
32. S. Li, X. Liu, X. Zhang, Y. Liu, *Catalysts*, 2025, **15**, 157.
33. S. Li, X. Liu, X. Zhang, Y. Wang, S. Chen, Y. Liu and Y. Zhang, *Catalysts*, 2024, **14**, 159.
34. Q. Yang, Y. Gu, Y. Liu, X. Wang, S. Li, J. Zhang, W. Liu, L. Zhang and Y. Zhang, *Chem. Commun.*, 2024, **60**, 13554-13557.
35. Y. Zhang, S. Li, J. Zhang, L.-D. Zhao, Y. Lin, W. Liu and F. Rosei, *Natl. Sci. Rev.*, 2024, **11**, nwae036.
36. S. Yang, A. Verdaguer-Casadevall, L. Arnarson, L. Silvioli, V. Čolić, R. Frydendal, J. Rossmeisl, I. Chorkendorff, I. E. L. Stephens, *ACS Catal.*, 2018, **8**, 4064-4081.
37. S. Siahrostami, S. J. Villegas, A. H. Bagherzadeh Mostaghimi, S. Back, A. B. Farimani, H. Wang, K. A. Persson, J. Montoya, *ACS Catal.,* 2020**, 10**, 7495-7511.
38. J. Wang, D. Kim, J. H. Park, S. Ryu, M. Shokouhimehr and H. W. Jang, *Energy Fuels*, 2023, **37**, 17629-17651.
39. A. Yu, S. Liu and Y. Yang, *Chem. Commun.*, 2024, **60**, 5232-5244.
40. Y. Wang, G. I. N. Waterhouse, L. Shang and T. Zhang, *Adv. Energy Mater.*, 2021, **11**, 2003323.
41. J. S. Jirkovský, I. Panas, E. Ahlberg, M. Halasa, S. Romani and D. J. Schiffrin, *J. Am. Chem. Soc.*, 2011, **133**, 19432-19441.
42. K. Gong, F. Du, Z. Xia, M. Durstock and L. Dai, *Science*, 2009, **323**, 760-764.
43. Q. Zhai, H. Huang, T. Lawson, Z. Xia, P. Giusto, M. Antonietti, M. Jaroniec, M. Chhowalla, J.-B. Baek, Y. Liu, S. Qiao and L. Dai, *Adv. Mater.*, **36**, 2405664.
44. H. W. Kim, M. B. Ross, N. Kornienko, L. Zhang, J. Guo, P. Yang and B. D. McCloskey, *Nat. Catal.*, 2018, **1**, 282-290.
45. J. Zhu, X. Xiao, K. Zheng, F. Li, G. Ma, H.-C. Yao, X. Wang and Y. Chen, *Carbon*, 2019, **153**, 6-11.
46. M. Niamlaem, C. Boonyuen, W. Sangthong, J. Limtrakul, D. Zigah, A. Kuhn and C. Warakulwit, *Carbon*, 2020, **170**, 154-164.
47. J. Biemolt, K. van der Veen, N. J. Geels, G. Rothenberg and N. Yan, *Carbon*, 2019, **155**, 643-649.
48. T.-N. Pham-Truong, T. Petenzi, C. Ranjan, H. Randriamahazaka and J. Ghilane, *Carbon*, 2018, **130**, 544-552.
49. A. R. Puente Santiago, O. Fernandez-Delgado, A. Gomez, M. A. Ahsan and L. Echegoyen, *Angew. Chem. Int. Ed.*, 2021, **60**, 122-141.
50. Y. Liu, X. Quan, X. Fan, H. Wang and S. Chen, *Angew. Chem. Int. Edit.*, 2015, **54**, 6837-6841.
51. L. Jing, W. Wang, Q. Tian, Y. Kong, X. Ye, H. Yang, Q. Hu and C. He, *Angew. Chem.*

View Article Online
DOI: 10.1039/D5MH00221D



*Int. Edit.*, 2024, **63**, e202403023.
52. J. S. Lim, J. H. Kim, J. Woo, D. S. Baek, K. Ihm, T. J. Shin, Y. J. Sa and S. H. Joo, *Chem*, 2021, **7**, 3114-3130.
53. L. Wei, Z. Dong, R. Chen, Q. Wu and J. Li, *Ionics*, 2022, **28**, 4045-4063.
54. Z.-y. Sang, F. Hou, S.-h. Wang and J. Liang, *Carbon*, 2022, **192**, 484.
55. Y.-Y. Yan, W.-J. Niu, W.-W. Zhao, R.-J. Li, E.-P. Feng, B.-X. Yu, B.-K. Chu and C.-Y. Cai, *Adv. Energy Mater.*, 2024, **14**, 2303506.
56. H. He, S. Liu, Y. Liu, L. Zhou, H. Wen, R. Shen, H. Zhang, X. Guo, J. Jiang and B. Li, *Green Chem.*, 2023, **25**, 9501-9542.
57. Z. Deng, S. J. Choi, G. Li and X. Wang, *Chem. Soc. Rev.*, 2024, **53**, 8137-8181.
58. H. He, S. Liu, Y. Liu, L. Zhou, H. Wen, R. Shen, H. Zhang, X. Guo, J. Jiang and B. Li, *Green Chem.*, 2023, **25**, 9501-9542
59. X. Shi, S. Siahrostami, G.-L. Li, Y. Zhang, P. Chakthranont, F. Studt, T. F. Jaramillo, X. Zheng and J. K. Nørskov, *Nat. Commun.*, 2017, **8**, 701.
60. L. Lin, L. Huang, C. Wu, Y. Gao, N. Miao, C. Wu, A. T. Marshall, Y. Zhao, J. Wang, J. Chen, S. Dou, G. G. Wallace and W. Huang, *Angew. Chem. Int. Ed.*, 2023, **62**, e202315182.
61. J. Su, L. Jiang, B. Xiao, Z. Liu, H. Wang, Y. Zhu, J. Wang and X. Zhu, *Small*, 2023, **20**, 2310317.
62. R. Xie, C. Cheng, R. Wang, J. Li, E. Zhao, Y. Zhao, Y. Liu, J. Guo, P. Yin and T. Ling, *ACS Catal.*, 2024, **14**, 4471-4477.
63. X. Luo, R. Zhu, L. Zhao, X. Gong, L. Zhang, L. Fan and Y. Liu, *Environ. Res.*, 2024, **251**, 118644.
64. Luo, S.; Elouarzaki, K.; Xu, Z. J., Electrochemistry in Magnetic Fields. *Angew. Chem. Int. Ed.*, 2022, **61**, e202203564.
65. X. Hu, Z. Sun, G. Mei, X. Zhao, B. Y. Xia and B. You, *Adv. Energy Mater.*, 2022, **12**, 2201466.
66. D. Kai, L. Jie, W. Yuanyuan, R. Yuchun, X. Zhaoquan, Z. Haiping, L. Lei, L. Qian, L. Yonglan, L. Tingshuai, M. A. Abdullah, L. Quan, M. Dongwei and S. Xuping, *Chem Catal.*, 2021, **1**, 1437-1448.
67. S. Mavrikis, M. Göltz, S. C. Perry, F. Bogdan, P. K. Leung, S. Rosiwal, L. Wang and C. Ponce de León, *ACS Energy Lett.*, 2021, **6**, 2369-2377.
68. Z. Chen, X. Liu, K. Wang, L. Yang, Y. Wang, X. Wang, S. Song, Z. Chen, *Adv. Funct. Mater.,* 2025, **35**, 2413243.
69. Y. Liang, Y. Han, J.-s. Li, Wang, J. D. Liu, Q. Fan, *J. Energy Chem.,* 2022, **70**, 643-655.
70. Y. Wang, Y. Xue, *ACS Appl. Nano Mater*., 2023, **6**, 23565-23575.
71. H. Zhang, Y. Zhao, Y. Li, G. Li, J. Li, F. Zhang, *ACS Appl. Energy Mater*., 2020, **3**, 705-714.
72. S. Sun, J. Dang, K. Ji, Z. Shi, M. Chen, C. Zhang, S. Liu, *Renew. Sust. Energ. Rev*., 2023, **183**, 113538.
73. Y. Jia and X. Yao, *Chem*, 2020, **6**, 548-550.
74. Q. Chang, P. Zhang, A. H. B. Mostaghimi, X. Zhao, S. R. Denny, J. H. Lee, H. Gao, Y. Zhang, H. L. Xin, S. Siahrostami, J. G. Chen and Z. Chen, *Nat. Commun.*, 2020, **11**, 2178.
75. F. Y. Yu, Y. J. Zhou, H. Q. Tan, Y. G. Li and Z. H. Kang, *Adv. Energy Mater.*, 2023, **13**, 2300119.
76. M. Deng, D. Wang and Y. Li, *Adv. Mater.*, 2024, **36**, 2314340.
77. N. Ramaswamy, U. Tylus, Q. Jia, S. Mukerjee, *J. Am. Chem. Soc*., 2013, **135**, 15443-15449.
78. N. Ramaswamy, SMukerjee, *Phys. Chem. C,* 2011, **115**, 18015-18026.

79. Y. Tang, B. L. Allen, D. R. Kauffman, A. Star, *J. Am. Chem. Soc*., 2009, **131**, 13200-13201.
80. T.-P. Fellinger, F. Hasché, P. Strasser, M. Antonietti, *J. Am. Chem. Soc*., 2012, **134**, 4072-4075.
81. Y. Pang, K. Wang, H. Xie, Y. Sun, M.-M. Titirici and G.-L. Chai, *ACS Catal.*, 2020, **10**, 7434-7442.
82. Y. Xia, X. Zhao, C. Xia, Z.-Y. Wu, P. Zhu, J. Y. Kim, X. Bai, G. Gao, Y. Hu, J. Zhong, Y. Liu and H. Wang, *Nat. Commun.*, 2021, **12**, 4225.
83. N. Wang, X. Zhao, R. Zhang, S. Yu, Z. H. Levell, C. Wang, S. Ma, P. Zou, L. Han, J. Qin, L. Ma, Y. Liu and H. L. Xin, *ACS Catal.*, 2022, **12**, 4156-4164.
84. Q. Tian, L. Jing, H. Du, Y. Yin, X. Cheng, J. Xu, J. Chen, Z. Liu, J. Wan, J. Liu and J. Yang, *Nat. Commun.*, 2024, **15**, 983.
85. L. Yang, H. Cheng, H. Li, G. Sun, S. Liu, T. Ma and L. Zhang, *Adv. Mater.*, 2024, **36,** 2406957.
86. Q. Tian, L. Jing, Y. Yin, Z. Liang, H. Du, L. Yang, X. Cheng, D. Zuo, C. Tang, Z. Liu, J. Liu, J. Wan and J. Yang, *Nano Lett.*, 2024, **24**, 1650-1659.
87. C. Du, P. Li, Z. Zhuang, Z. Fang, S. He, L. Feng and W. Chen, *Coordin. Chem. Rev.*, 2022, **466**, 214604.
88. L. Kořená, V. Slovák, G. Zelenková and T. Zelenka, *Carbon*, 2023, **206**, 303-313.
89. A. Wang, Y. Ma and D. Zhao, *ACS Nano*, 2024, **18**, 22829-22854.
90. L. Jing, Q. Tian, W. Wang, X. Li, Q. Hu, H. Yang and C. He, *Adv. Energy Mater.*, 2024, **14**, 2304418.
91. Y. Hu, J. Zhang, T. Shen, Z. Li, K. Chen, Y. Lu, J. Zhang and D. Wang, *ACS Appl. Mater. Interfaces*, 2021, **13**, 29551-29557.
92. J. Xi, S. Yang, L. Silvioli, S. Cao, P. Liu, Q. Chen, Y. Zhao, H. Sun, J. N. Hansen, J.-P. B. Haraldsted, J. Kibsgaard, J. Rossmeisl, S. Bals, S. Wang and I. Chorkendorff, *J. Catal.*, 2021, **393**, 313-323.
93. C. Qi, W. Bao, J. Xu, Y. Li, F. Xu, M. Li, L. Wang, W. Jiang, P. Qiu and W. Luo, *Angew. Chem. Int. Ed.*, 2025, e202500177. doi: 10.1002/anie.202500177.
94. W. Zhu, Z. Chen, Y. Pan, R. Dai, Y. Wu, Z. Zhuang, D. Wang, Q. Peng, C. Chen and Y. Li, *Adv. Mater.*, 2019, **31**, 1800426.
95. Z. Yu, N. Ji, X. Li, R. Zhang, Y. Qiao, J. Xiong, J. Liu and X. Lu, *Angew. Chem. Int. Ed.*, 2023, **62**, e202213612.
96. X. Tang, Y. Wei, W. Zhai, Y. Wu, T. Hu, K. Yuan and Y. Chen, *Adv. Mater.*, 2023, **35**, 2208942.
97. Y. Bu, Y. Wang, G.-F. Han, Y. Zhao, X. Ge, F. Li, Z. Zhang, Q. Zhong and J.-B. Baek, *Adv. Mater.*, 2021, **33**, 2103266.
98. J. Zhu and S. Mu, *Adv. Funct. Mater.*, 2020, **30**, 2001097.
99. L. Jing, Q. Tian, X. Li, J. Sun, W. Wang, H. Yang, X. Chai, Q. Hu and C. He, *Adv. Funct. Mater.*, 2023, **33**, 2305795.
100. Z. Mou, Y. Mu, L. Liu, D. Cao, S. Chen, W. Yan, H. Zhou, T.-S. Chan, L.-Y. Chang and X. Fan, *Small*, 2024, **20**, 2400564.
101. C. Zhang, C. Wu, L. Wang and G. Liu, *ACS Appl. Mater. Interfaces*, 2023, **15**, 838-847.
102. J. Zhu, Y. Huang, W. Mei, C. Zhao, C. Zhang, J. Zhang, I. S. Amiinu and S. Mu, *Angew. Chem. Int. Ed.*, 2019, **58**, 3859-3864.
103. C. Zhang, W. Shen, K. Guo, M. Xiong, J. Zhang and X. Lu, *J. Am. Chem. Soc.*, 2023, **145**, 11589-11598.
104. L. Lin, L. Huang, C. Wu, Y. Gao, N. Miao, C. Wu, A. T. Marshall, Y. Zhao, J. Wang, J. Chen, S. Dou, G. G. Wallace and W. Huang, *Angew. Chem. Int. Ed.*, 2023, **62**, e202315182.
105. D. San Roman, D. Krishnamurthy, R. Garg, H. Hafiz, M. Lamparski, N. T. Nuhfer, V.

Meunier, V. Viswanathan and T. Cohen-Karni, *ACS Catal.*, 2020, **10**, 1993-2008.
106. Y. J. Sa, J. H. Kim and S. H. Joo, *Angew. Chem. Int. Ed.*, 2019, **58**, 1100-1105.
107. F. She, Z. Guo, F. Liu, Z. Yu, J. Chen, Y. Fan, Y. Lei, Y. Chen, H. Li and L. Wei, *ACS Catal.*, 2024, **14**, 10928-10938.
108. X. Wang, C. Han, Y. Han, R. Huang, H. Sun, P. Guo, X. Liu, M. Huang, Y. Chen, H. Wu, J. Zhang, X. Yan, Z. Mao, A. Du, Y. Jia and L. Wang, *Small*, 2024, **20**, 2401447.
109. W. Shen, C. Zhang, M. Alomar, Z. Du, Z. Yang, J. Wang, G. Xu, J. Zhang, J. Lv and X. Lu, *Nano Res.*, 2024, **17**, 1217-1224.
110. M. Fan, Z. Wang, K. Sun, A. Wang, Y. Zhao, Q. Yuan, R. Wang, J. Raj, J. Wu, J. Jiang and L. Wang, *Adv. Mater.*, 2023, **35**, 2209086.
111. J. W. Choi, A. Byeon, S. Kim, C.-K. Hwang, W. Zhang, J. Lee, W. C. Yun, S. Y. Paek, J. H. Kim, G. Jeong, S. Y. Lee, J. Moon, S. S. Han, J. W. Lee and J. M. Kim, *Adv. Mater.*, 2025, doi: 10.1002/adma.202415712.
112. N. Wang, S. Ma, R. Zhang, L. Wang, Y. Wang, L. Yang, J. Li, F. Guan, J. Duan and B. Hou, *Adv. Sci.*, 2023, **10**, 2302446.
113. Z. Xing, K. Shi, Z. S. Parsons and X. Feng, *ACS Catal.*, 2023, **13**, 2780-2789.
114. L. Xie, C. Liang, Y. Wu, K. Wang, W. Hou, H. Guo, Z. Wang, Y. M. Lam, Z. Liu and L. Wang, *Small*, **20**, 2401253.
115. W. Shen, C. Zhang, X. Wang, Y. Huang, Z. Du, M. Alomar, J. Wang, J. Lv, J. Zhang and X. Lu, *ACS Materials Lett.*, 2024, **6**, 17-26.
116. H. Jiang, Y. Wang, J. Hao, Y. Liu, W. Li and J. Li, *Carbon*, 2017, **122**, 64-73.
117. Y. Wu, Z. Gao, Y. Feng, Q. Cui, C. Du, C. Yu, L. Liang, W. Zhao, J. Feng, J. Sun, R. Yang and J. Sun, *Appl. Catal. B-Environ.*, 2021, **298**, 120572.
118. C. Ma, Q. Hao, J. Hou, A. Liu and X. Xiang, *Carbon Res.*, 2024, **3**, 5.
119. G.-F. Han, F. Li, W. Zou, M. Karamad, J.-P. Jeon, S.-W. Kim, S.-J. Kim, Y. Bu, Z. Fu, Y. Lu, S. Siahrostami and J.-B. Baek, *Nat. Commun.*, 2020, **11**, 2209.
120. X. Shen, Z. Wang, H. Guo, Z. Lei, Z. Liu and L. Wang, *Small*, 2023, **19**, 2303156.
121. Q. Wu, H. Zou, X. Mao, J. He, Y. Shi, S. Chen, X. Yan, L. Wu, C. Lang, B. Zhang, L. Song, X. Wang, A. Du, Q. Li, Y. Jia, J. Chen and X. Yao, *Nat. Commun.*, 2023, **14**, 6275.
122. J. Qu, G. Long, L. Luo, Y. Yang, W. Fan and F. Zhang, *Small*, 2024, **20**, 2400695.
123. X. Wen, X. Zhang, M. Wang, C. Yuan, J. Lang, X. Li, H. Wei, D. Mandler and M. Long, *Appl. Catal. B-Environ.*, 2024, **342**, 123437.
124. G. Alemany-Molina, J. Fernández-Catalá, W. Cao, E. Morallón and D. Cazorla-Amorós, *Mater. Today Chem.*, 2024, **35**, 101858.
125. A. Zhang, Y. Liu, J. Wu, J. Zhu, S. Cheng, Y. Wang, Y. Hao and S. Zeng, *Chem. Eng. J.*, 2023, **454**, 140317.
126. A. B. Trench, J. Paulo C. Moura, V. S. Antonin, C. Machado Fernandes, L. Liu and M. C. Santos, *Adv. Powder Technol.*, 2024, **35**, 104404.
127. M. A. Rashed, M. Faisal, F. A. Harraz, M. Jalalah, M. Alsaiari and S. A. Alsareii, *J. Electrochem. Soc.*, 2021, **168**, 027512.
128. B. Yu, J. Diniz, K. Lofgren, Q. Liu, R. Mercado, F. Nichols, S. R. J. Oliver and S. Chen, *ACS Sustain. Chem. Eng.*, 2022, **10**, 15501-15507.
129. C. Guo, Y. Ruan, S. Zhang, L. Kan, H. Bian, F. Rong, L. He, D. Li, M. Du and Z. Zhang, *Chem. Eng. J.*, 2023, **466**, 143033.
130. N. Cheng, S. Stambula, D. Wang, M. N. Banis, J. Liu, A. Riese, B. Xiao, R. Li, T.-K. Sham, L.-M. Liu, G. A. Botton and X. Sun, *Nat. Commun.*, 2016, **7**, 13638.
131. Q. Chang, P. Zhang, A. H. B. Mostaghimi, X. Zhao, S. R. Denny, J. H. Lee, H. Gao, Y. Zhang, H. L. Xin, S. Siahrostami, J. G. Chen and Z. Chen, *Nat. Commun.*, 2020, **11**, 2178.
132. C. Jing, J. Ding, P. Jia, M. Jin, L. Zhou, X. Liu, J. Luo and S. Dai, *Carbon Energ.*, 2024,

View Article Online
DOI: 10.1039/D5MH00221D



**6**, e581.
133. G. Wei, Y. Li, X. Liu, J. Huang, M. Liu, D. Luan, S. Gao and X. W. Lou, *Angew. Chem. Int. Ed.*, 2023, **62**, e202313914.
134. C. Xiao, L. Cheng, Y. Zhu, G. Wang, L. Chen, Y. Wang, R. Chen, Y. Li and C. Li, *Angew. Chem. Int. Ed.*, 2022, **61**, e202206544.
135. M. Deng, D. Wang and Y. Li, *Adv. Mater.*, 2024, **36**, 2314340.
136. Y.-X. Du, Q. Yang, W.-T. Lu, Q.-Y. Guan, F.-F. Cao and G. Zhang, *Adv. Funct. Mater.*, 2023, **33**, 2300895.
137. M. Song, W. Liu, J. Zhang, C. Zhang, X. Huang and D. Wang, *Adv. Funct. Mater.*, 2023, **33**, 2212087.
138. H. Gong, Z. Wei, Z. Gong, J. Liu, G. Ye, M. Yan, J. Dong, C. Allen, J. Liu, K. Huang, R. Liu, G. He, S. Zhao and H. Fei, *Adv. Funct. Mater.*, 2022, **32**, 2106886.
139. C.-K. Hwang, S. Kim, K. R. Yoon, T. T. Le, C. V. Hoang, J. W. Choi, W. Zhang, S. Y. Paek, C. H. Lee, J. H. Lee, K. H. Chae, S. Jeong, S. Y. Lee, B.-K. Ju, S. H. Kim, S. S. Han and J. M. Kim, *Carbon Energ.*, 2024, **6**, e582.
140. S. Zhang, Z. Tao, M. Xu, L. Kan, C. Guo, J. Liu, L. He, M. Du and Z. Zhang, *Small*, 2024, **20**, 2310468.
141. C. Tang, L. Chen, H. Li, L. Li, Y. Jiao, Y. Zheng, H. Xu, K. Davey and S.-Z. Qiao, *J. Am. Chem. Soc.*, 2021, **143**, 7819-7827.
142. H. Xu, S. Zhang, X. Zhang, M. Xu, M. Han, L. R. Zheng, Y. Zhang, G. Wang, H. Zhang and H. Zhao, *Angew. Chem. Int. Ed.*, 2023, **62**, e202314414.
143. L.-Y. Dong, J.-S. Wang, T.-Y. Li, T. Wu, X. Hu, Y.-T. Wu, M.-Y. Zhu, G.-P. Hao and A.-H. Lu, *Angew. Chem. Int. Ed.*, 2024, **63**, e202317660.
144. F. Zhang, Y. Zhu, C. Tang, Y. Chen, B. Qian, Z. Hu, Y.-C. Chang, C.-W. Pao, Q. Lin, S. A. Kazemi, Y. Wang, L. Zhang, X. Zhang and H. Wang, *Adv. Funct. Mater.*, 2022, **32**, 2110224.
145. H. Yang, N. Lu, J. Zhang, R. Wang, S. Tian, M. Wang, Z. Wang, K. Tao, F. Ma and S. Peng, *Carbon Energ.*, 2023, **5**, e337.
146. J. H. Kim, D. Shin, J. Lee, D. S. Baek, T. J. Shin, Y.-T. Kim, H. Y. Jeong, J. H. Kwak, H. Kim and S. H. Joo, *ACS Nano*, 2020, **14**, 1990-2001.
147. X. Zhou, Y. Min, C. Zhao, C. Chen, M.-K. Ke, S.-L. Xu, J.-J. Chen, Y. Wu and H.-Q. Yu, *Nat. Commun.*, 2024, **15**, 193.
148. Y. Gu, Y. Tan, H. Tan, Y. Han, D. Cheng, F. Lin, Z. Qian, L. Zeng, S. Zhang, R. Zeng, Y. Liu, H. Guo, M. Luo and S. Guo, *Nat. Synth.*, 2025, **4**, 857.
149. E. Zhang, L. Tao, J. An, J. Zhang, L. Meng, X. Zheng, Y. Wang, N. Li, S. Du, J. Zhang, D. Wang and Y. Li, *Angew. Chem. Int. Ed.*, 2022, **61**, e202117347.
150. J. Gao, H. b. Yang, X. Huang, S.-F. Hung, W. Cai, C. Jia, S. Miao, H. M. Chen, X. Yang, Y. Huang, T. Zhang and B. Liu, *Chem*, 2020, **6**, 658-674.
151. J. Du, G. Han, W. Zhang, L. Li, Y. Yan, Y. Shi, X. Zhang, L. Geng, Z. Wang, Y. Xiong, G. Yin and C. Du, *Nat. Commun.*, 2023, **14**, 4766.
152. A. I. M. Albashir, X. Lu, X. Dai, W. Qi, *Commun. Chem*., 2024, **7**, 111.
153. M. Yang, W. Song, C. Chen, X.Yang, Z. Zhuang, H. Zhang, F. Wang, L. Yu, *Adv. Mater.*, 2025, 2416401, doi.org/10.1002/adma.202416401.
154. C. Liu, H. Tong, P. Wang, P. Huang, Z. Yang, R. Huang and G. Zhou, *Chem. Eng. J.*, 2023, **476**, 146573.
155. Y. Wang, Y. Zhou, Y. Feng and X. Y. Yu, *Adv. Funct. Mater.*, 2022, **32**, 2110734.
156. T. C. Nagaiah, D. Schäfer, W. Schuhmann, N. Dimcheva, *Anal. Chem.* 2013, **85**, 7897-7903.
157. Y. Chang, J. Yang, M. Zhang, M. Yue, W. Wang, J. Li, J. Wang, K. Song, Y. Liu, Y. Zuo, R. Xing, *J. Alloy. Compd*., 2024, **1005**, 176091.
158. R. Gao, L. Pan, Z. Li, C. Shi, Y. Yao, X. Zhang, J.-J. Zou, *Adv. Funct. Mater*., 2020,

View Article Online
DOI: 10.1039/D5MH00221D

**30**, 1910539.
159. Y. Zhang, M. Wang, W. Zhu, M. Fang, M. Ma, F. Liao, H. Yang, T.Cheng, C.-W. Pao, Y.-C. Chang, Z. Hu, Q. Shao, M.Shao, Z. Kang, *Angew. Chem. Int. Ed.*, 2023, **62**, e202218924.
160. H. Li, P. Wen, D. S. Itanze, Z. D. Hood, S. Adhikari, C. Lu, X. Ma, C. Dun, L. Jiang, D. L. Carroll, Y. Qiu, S. M. Geyer, *Nat. Commun*., 2020, **11**, 3928.
161. R. Shen, W. Chen, Q. Peng, S. Lu, L. Zheng, X. Cao, Y. Wang, W. Zhu, J. Zhang, Z. Zhuang, C. Chen, D. Wang, Y. Li, *Chem*, 2019, **5**, 2099-2110.
162. X.-D. Zhu, Q. Zhang, X. Yang, Y. Wang, J. Wu, J. Gao, J.-J. Zou, G. Wu, Y.-C. Zhang, *SusMat*, 2023, **3**, 334-344.
163. H. Xu, S. Zhang, X. Zhang, M. Xu, M. Han, L. R. Zheng, Y. Zhang, G. Wang, H. Zhang and H. Zhao, *Angew. Chem. Int. Edit.*, 2023, **62**, e202314414.
164. Y. Long, J. Lin, F. Ye, W. Liu, D. Wang, Q. Cheng, R. Paul, D. Cheng, B. Mao, R. Yan, L. Zhao, D. Liu, F. Liu and C. Hu, *Adv. Mater.*, 2023, **35**, 2303905.
165. A. Byeon, J. W. Choi, H. W. Lee, W. C. Yun, W. Zhang, C.-K. Hwang, S. Y. Lee, S. S. Han, J. M. Kim and J. W. Lee, *Appl. Catal. B-Environ.*, 2023, **329**, 122557.
166. M. Wang, N. Zhang, Y. Feng, Z. Hu, Q. Shao, X. Huang, *Angew. Chem. Int. Ed.*, 2020, **59**, 14373-14377.
167. Y. Wu, Y. Zhao, Q. Yuan, H. Sun, A. Wang, K. Sun, G. I. N. Waterhouse, Z. Wang, J. Wu, J. Jiang, M. Fan, *Nat. Commun.* 2024, **15**, 10843.
168. Q. Tian, L. Jing, H. Du, Y. Yin, X. Cheng, J. Xu, J. Chen, Z. Liu, J. Wan, J. Liu and J. Yang, *Nat. Commun.*, 2024, **15**, 983.
169. L. June Sung, K. Jae Hyung, W. Jinwoo, B. Du San, I. Kyuwook, S. Tae Joo, S. Young Jin and J. Sang Hoon, *Chem*, 2021, **7**, 3114-3130.
170. Y. J. Sa, J. H. Kim and S. H. Joo, *Angew. Chem. Int. Ed.*, 2018, **58**, 1100-1105.
171. K. Dong, J. Liang, Y. Wang, Z. Xu, Q. Liu, Y. Luo, T. Li, L. Li, X. Shi, A. M. Asiri, Q. Li, D. Ma and X. Sun, *Angew. Chem. Int. Ed.*, 2021, **60**, 10583-10587.
172. L. Liu, L. Kang, A. Chutia, J. Feng, M. Michalska, P. Ferrer, D. C. Grinter, G. Held, Y. Tan, F. Zhao, F. Guo, D. G. Hopkinson, C. S. Allen, Y. Hou, J. Gu, I. Papakonstantinou, P. R. Shearing, D. J. L. Brett, I. P. Parkin and G. He, *Angew. Chem. Int. Ed.*, 2023, **62**, e202303525.
173. D. Zhiping and W. Xiaolei, *Nano Res.*, 2022, **15**, 4599-4605.
174. L. Jing, Q. Tian, X. Li, J. Sun, W. Wang, H. Yang, X. Chai, Q. Hu and C. He, *Adv. Funct. Mater.*, 2023, **33**, 2305795.
175. K. H. Koh, A. H. Bagherzadeh Mostaghimi, Q. Chang, Y. J. Kim, S. Siahrostami, T. H. Han and Z. Chen, *EcoMat*, 2023, **5**, e12266.
176. F. She, Z. Guo, F. Liu, Z. Yu, J. Chen, Y. Fan, Y. Lei, Y. Chen, H. Li and L. Wei, *ACS Catal.*, 2024, **14**, 10928-10938.
177. L. Xie, C. Liang, Y. Wu, K. Wang, W. Hou, H. Guo, Z. Wang, Y. M. Lam, Z. Liu and L. Wang, *Small*, 2024, **20**, e2401253.
178. Q. Wu, H. Zou, X. Mao, J. He, Y. Shi, S. Chen, X. Yan, L. Wu, C. Lang, B. Zhang, L. Song, X. Wang, A. Du, Q. Li, Y. Jia, J. Chen and X. Yao, *Nat. Commun.*, 2023, **14**, 6275.
179. P. Chakthranont, S. Nitrathorn, S. Thongratkaew, P. Khemthong, H. Nakajima, R. Supruangnet, T. Butburee, N. Sano and K. Faungnawakij, *ACS Appl. Energy Mater.*, 2021, **4**, 12436-12447.
180. W. Shen, C. Zhang, M. Alomar, Z. Du, Z. Yang, J. Wang, G. Xu, J. Zhang, J. Lv and X. Lu, *Nano Res.*, 2023, **17**, 1217-1224.
181. Y. Xia, X. Zhao, C. Xia, Z.-Y. Wu, P. Zhu, J. Y. T. Kim, X. Bai, G. Gao, Y. Hu, J. Zhong, Y. Liu and H. Wang, *Nat. Commun.*, 2021, **12**, 4225.
182. Y. Hu, J. Zhang, T. Shen, Z. Li, K. Chen, Y. Lu, J. Zhang and D. Wang, *ACS Appl.*

View Article Online
DOI: 10.1039/D5MH00221D



*Mater. Interfaces*, 2021, **13**, 29551-29557.

183. L. Han, Y. Sun, S. Li, C. Cheng, C. E. Halbig, P. Feicht, J. L. Hübner, P. Strasser and S. Eigler, *ACS Catal.*, 2019, **9**, 1283-1288.
184. C. Zhang, W. Shen, K. Guo, M. Xiong, J. Zhang and X. Lu, *J. Am. Chem. Soc.*, 2023, **145**, 11589-11598.
185. N. Wang, S. Ma, R. Zhang, L. Wang, Y. Wang, L. Yang, J. Li, F. Guan, J. Duan and B. Hou, *Adv. Sci.*, 2023, **10**, 2302446.
186. L. Jing, Q. Tian, W. Wang, X. Li, Q. Hu, H. Yang and C. He, *Adv. Energy Mater.*, 2024, **14**, 2304418.
187. Y. Liu, S. Liu, J. Jiang, X. Wei, K. Zhao, R. Shen, X. Wang, M. Wei, Y. Wang, H. Pang, B. Li, *Adv. Mater*., 2025, 2502197. doi.org/10.1002/adma.202502197.
188. H. Gong, L. Wei, S. Chen, Z. Chen, T. F. Jaramillo and Z. Bao, *Nano Res.*, 2023, **16**, 11556-11563.
189. K.-H. Wu, D. Wang, X. Lu, X. Zhang, Z. Xie, Y. Liu, B.-J. Su, J.-M. Chen, D.-S. Su, W. Qi and S. Guo, *Chem*, 2020, **6**, 1443-1458.
190. C. Yang, F. Sun, Z. Qu, X. Li, W. Zhou, J. Gao, *ACS Energy Lett.* 2022, **7**, 4398-4407
191. M. Fan, Z. Wang, K. Sun, A. Wang, Y. Zhao, Q. Yuan, R. Wang, J. Raj, J. Wu, J. Jiang and L. Wang, *Adv. Mater.*, 2023, **35**, 2209086.
192. X. Zhou, Y. Min, C. Zhao, C. Chen, M.-K. Ke, S.-L. Xu, J.-J. Chen, Y. Wu and H.-Q. Yu, *Nat. Commun.*, 2024, **15**, 193.
193. E. Zhang, L. Tao, J. An, J. Zhang, L. Meng, X. Zheng, Y. Wang, N. Li, S. Du, J. Zhang, D. Wang and Y. Li, *Angew. Chem. Int. Ed.*, 2022, **61**, e202117347.
194. H. Yang, N. Lu, J. Zhang, R. Wang, S. Tian, M. Wang, Z. Wang, K. Tao, F. Ma, Peng, S., *Carbon Energy*, 2023, **5**, e337.
195. J. Shen, Y. Wen, H. Jiang, S. Yu, C. Dong, Y. Fan, B. Liu and C. Li, J. Phys. Chem.C, 2022, **126**, 10388-10398.
196. L. Yang, H. Cheng, H. Li, G. Sun, S. Liu, T. Ma and L. Zhang, *Adv. Mater.*, 2024, **36**, 2406957.
197. S. Zhang, Z. Tao, M. Xu, L. Kan, C. Guo, J. Liu, L. He, M. Du and Z. Zhang, *Small*, 2024, **20**, 2310468.
198. H. Gong, Z. Wei, Z. Gong, J. Liu, G. Ye, M. Yan, J. Dong, C. Allen, J. Liu, K. Huang, R. Liu, G. He, S. Zhao and H. Fei, *Adv. Funct. Mater.*, 2021, **32**, 2106886.
199. H. Gong, Z. Gong, J. Liu, G. Ye and H. Fei, *Adv. Funct. Mater.*, 2024, **34**, 2316438.
200. W. Liu, R. Chen, Z. Sang, Z. Li, J. Nie, L. Yin, F. Hou and J. Liang, *Adv. Mater.*, 2024, **36**, 2406403.
201. E. A. Moges, C.-Y. Chang, W.-H. Huang, F. T. Angerasa, K. Lakshmanan, T. M. Hagos, H. G. Edao, W. B. Dilebo, C.-W. Pao, M.-C. Tsai, W.-N. Su and B. J. Hwang, *J. Am. Chem. Soc.*, 2023, **12**, 4156-4164.
202. N. Wang, X. Zhao, R. Zhang, S. Yu, Z. H. Levell, C. Wang, S. Ma, P. Zou, L. Han, J. Qin, L. Ma, Y. Liu and H. L. Xin, *ACS Catal.*, 2022, **12**, 4156-4164.
203. G. Wei, Y. Li, X. Liu, J. Huang, M. Liu, D. Luan, S. Gao and X. W. D. Lou, *Angew. Chem. Int. Ed.*, 2023, **62**, e202313914.
204. C. K. Hwang, S. Kim, K. R. Yoon, T. T. Le, C. V. Hoang, J. W. Choi, W. Zhang, S. Y. Paek, C. H. Lee, J. H. Lee, K. H. Chae, S. Jeong, S. Y. Lee, B. K. Ju, S. H. Kim, S. S. Han and J. M. Kim, *Carbon Energ.*, 2024, **6**, e582.
205. F. Zhang, Y. Zhu, C. Tang, Y. Chen, B. Qian, Z. Hu, Y. C. Chang, C. W. Pao, Q. Lin, S. A. Kazemi, Y. Wang, L. Zhang, X. Zhang and H. Wang, *Adv. Funct. Mater.*, 2021, **32**, 2110224.
206. C. Zhang, C. Wu, L. Wang and G. Liu, *ACS Appl. Mater. Interfaces*, 2023, **15**, 838-847.
207. Y. Wang, Y. Zhou, Y. Feng, X. Y. Yu, *Adv. Funct. Mater*., 2022, **32**, 2110734.
208. C. Xiao, L. Cheng, Y. Zhu, G. Wang, L. Chen, Y. Wang, R. Chen, Y. Li and C. Li,

View Article Online
DOI: 10.1039/D5MH00221D

*Angew. Chem. Int. Ed.*, 2022, **61**, e202206544.

209. W. Yuhan, G. Zhixiao, F. Yiran, C. Qiannan, D. Cuiwei, Y. Chongfei, L. Liang, Z. Wen, F. Jinglan, S. Jianhui, Y. Ruizhi and S. Jingyu, *Appl. Catal. B-Environ.*, 2021, **298**, 120572.

210. C. Yang, F. Sun, Z. Qu, X. Li, W. Zhou and J. Gao, *ACS Energy Lett.*, 2022, **7**, 4398-4407.

211. Y. Xia, P. Zhu, Y.Yang, C. Qiu, H. Wang, *ACS Catal.*, 2025, **15**, 4560-4569.

212. J. Wang, J. Li, Z. Li, J. Wu, H. Si, Y. Wu, Z. Guo, X. Wang, F. Liao, H. Huang, M. Shao, Y. Liu and Z. Kang, *Nano Res.*, 2024, **17**, 5956-5964.

213. D. Oh, S. W. Hwang, D. Y. Kim, J. E. Matthews, J. Lee, J. E. A. Acosta, S.-W. Lee, Y. Xu, A. Cho, D. U. Lee, T. F. Jaramillo, D.-H. Seo, J.-W. Jang, *Nat. Synth*., 2025, doi.org/10.1038/s44160-025-00774-y.

214. K. Yu, S. Guan, W. Zhang, W. Zhang, Y. Meng, H. Lin, Q. Gao, *Angew. Chem. Int. Edit.*, 2025, e202502383. doi.org/10.1002/anie.202502383.